

# Classifying World War II Era Ciphers with Machine Learning

Brooke Dalton\* Mark Stamp\*†

July 4, 2023

## Abstract

We determine the accuracy with which machine learning and deep learning techniques can classify selected World War II era ciphers when only ciphertext is available. The specific ciphers considered are **Enigma**, **M-209**, **Sigaba**, **Purple**, and **Typex**. We experiment with three classic machine learning models, namely, Support Vector Machines (SVM),  $k$ -Nearest Neighbors ( $k$ -NN), and Random Forest (RF). We also experiment with four deep learning neural network-based models: Multi-Layer Perceptrons (MLP), Long Short-Term Memory (LSTM), Extreme Learning Machines (ELM), and Convolutional Neural Networks (CNN). Each model is trained on features consisting of histograms, digrams, and raw ciphertext letter sequences. Furthermore, the classification problem is considered under four distinct scenarios: Fixed plaintext with fixed keys, random plaintext with fixed keys, fixed plaintext with random keys, and random plaintext with random keys. Under the most realistic scenario, given 1000 characters per ciphertext, we are able to distinguish the ciphers with greater than 97% accuracy. In addition, we consider the accuracy of a subset of the learning techniques as a function of the length of the ciphertext messages. Somewhat surprisingly, our classic machine learning models perform at least as well as our deep learning models. We also find that ciphers that are more similar in design are somewhat more challenging to distinguish, but not as difficult as might be expected.

## 1 Introduction

Many cipher machines were created and utilized by various nations during World War II. For example, the **Enigma** is a rotor-based cipher machine that was invented as a commercial product and was later modified and deployed by the German military. Other rotor-based cipher machines of the same era include the **M-209 Converter** (henceforth, simply referred to as **M-209**) and **Sigaba**, which

---

\*Department of Computer Science, San Jose State University

†mark.stamp@sjsu.edu

were both created by the United States, and the British-built **Typex**. The well-known **Purple** cipher machine that was used by Japan in World War II employed a switch-based system. Although these ciphers have all been broken [4, 5, 9, 20], and cryptography has improved significantly since World War II, accurately classifying ciphertext generated by these machines is an interesting challenge. There has been previous research on classifying classic ciphers by applying machine learning techniques [13], but as far as the authors are aware, to date no such work has focused on the WWII-era ciphers considered in this paper.

Our research examines whether machine learning and deep learning techniques can classify selected World War II era ciphers when only ciphertext is provided. We consider the five ciphers mentioned above, namely, **Enigma**, **M-209**, **Purple**, **Sigaba**, and **Typex**. For each cipher, we train and test machine learning techniques based on a variety of features; specifically, the raw ciphertext letter sequence, letter histograms, and letter digram statistics. We experiment with three popular classic machine learning techniques, namely, Support Vector Machines (SVM),  $k$ -Nearest Neighbors ( $k$ -NN), and Random Forest (RF) models. Additionally, we experiment with four deep learning techniques, namely, Multi-Layer Perceptrons (MLP), Long Short-Term Memory (LSTM) models, Extreme Learning Machines (ELM), and Convolutional Neural Networks (CNN). We train and test models under four distinct scenarios, and we find that in the most realistic case, given sufficient ciphertext, we can identify the correct cipher machine with accuracy in excess of 97%. We also conduct experiments to determine the relationship between the ciphertext length and the accuracy of our various models.

The remainder of this paper is organized as follows. Section 2 considers relevant previous work and covers background topics, including an overview to the ciphers considered and an introduction to the machine learning algorithms that we use. In Section 3, we discuss our experimental setup, including how the dataset was created, along with feature extraction. Section 4 contains our experimental results, and we provide context and discussion of these results. In Section 5, we give our conclusions and discuss possible directions for future work.

## 2 Background

In this section, we briefly review the history of the ciphers used in our experiments, including an overview of their physical layout, as well as their cryptographically significant components. We also introduce the machine learning algorithms that we employ in our experiments.

### 2.1 World War II Ciphers

As mentioned above, in our experiments, we consider five World War II era ciphers. World War II was noteworthy for the application of cryptographic technology. The volume of data that was need for secure military communications

was much greater than in previous conflicts, and hence machine encryption was widely used for the first time. Before these machines, codebooks were often used for military purposes. While well-designed codebooks can be reasonably secure, they are cumbersome and slow.

Two of the five ciphers that we consider were used by the Axis powers, while the remaining three ciphers were used by the Allies. Both the Axis and Allied powers had confidence in the security of their cipher machines, yet there were major cryptanalytic successes during the war, especially by the Allies.

### 2.1.1 Enigma

The **Enigma** cipher machine is a rotor-based cipher that was invented by German engineer Arthur Scherbius. During World War II, the German military used modified versions of original **Enigma** machine, and it became their primary military cipher system and it was used throughout the war. The version of the cipher machine that we consider appears in Figure 1. This cipher has three rotors at the top, a keyboard for input, a lightboard to indicate the output, and a plugboard which is generally referred to by the German “stecker.” For our purposes, the key for this cipher consists of the initial rotor positions and stecker connections, although various other internal setting can be changed.



Figure 1: **Enigma** cipher machine [6]

A diagram illustrating the cryptographic elements of **Enigma** is given in Figure 2. In this illustrated example, the letter *C* is pressed on the keyboard, a stecker cable happens to map *C* to *S*, which is then passed through the stators (i.e., “static rotors” that do not rotate), the three rotors, and the reflector, then back through the rotors and stators, yielding the letter *Z*, which is mapped to *L* by the stecker. Finally, the letter *L* appears on the lightboard.

With each keyboard letter that is pressed, the fast rotor *F* steps once, while the medium rotor *M* steps once for each revolution of the fast rotor, and the slow rotor *S* steps once for each revolution of the medium rotor<sup>1</sup>.

---

<sup>1</sup>There is one slight quirk to the rotor stepping described here. When a rotor steps, it causes the

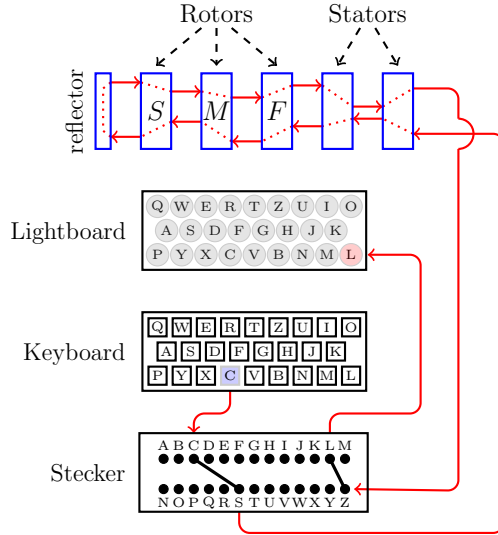


Figure 2: Enigma cipher diagram

The crucial cryptographic components of the **Enigma** are the rotors, stators, and the stecker. Each rotor consists of a hardwired mapping between letters—when a rotor steps, it has the effect of changing the overall permutation. Hence, the **Enigma** is a polyalphabetic substitution, with the current “alphabet” (i.e., permutation) determined by the configuration of the rotors. Note that the **Enigma** is an electro-mechanical device, which implies that the reflector permutation cannot have any fixed points, as a letter mapped to itself by the reflector would cause a short circuit. It is also interesting to note that the **Enigma** is self-inverse, and hence there is no need for separate encryption and decryption modes.

### 2.1.2 M-209

The M-209 Converter, as shown in Figure 3, is a mechanical rotor-based machine invented by Swedish engineer Boris Hagelin. This cipher was used by the United States military, and it is known as a “lug and pin” machine, for reasons that will become clear momentarily. The cipher includes six rotors, with the rotors from left to right containing 26, 25, 23, 21, 19, and 17 letters, respectively. Each rotor letter has a small pin that can be set to an active or inactive position. Behind the rotors is a cylindrical drum with 27 bars and two movable lugs per bar. There is an encoder wheel on the left of the machine with the alphabet on it—the alphabet also appears in reverse order on a smaller wheel. When encrypting or decrypting, a handle on the right of the machine is turned, which

---

rotor to its right to also step. Since the rightmost rotor steps with each letter pressed, when the *M* rotor steps, this quirk has no effect on the fast rotor. However, when the slow rotor steps, it causes the *M* rotor to step, which results in a “double stepping” condition. Thus, the period of the rotor stepping is  $26 \times 25 \times 26 \approx 2^{14.04}$ , not  $26^3 \approx 2^{14.10}$ .

causes the drum lugs to interact with the rotor pins. In practice, the settings of the lugs and pins was a daily key, while the message indicator (MI) consisted of the initial rotor settings.

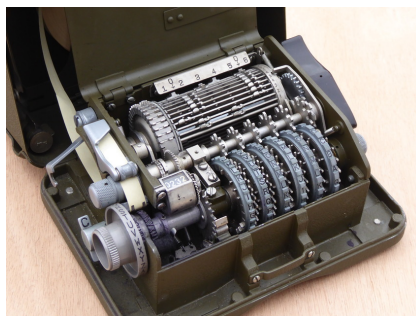


Figure 3: M-209 cipher machine [15]

A diagram illustrating the cryptographic components of M-209 is given in Figure 4. To encrypt a letter, the encoder wheel is turned so that the plaintext letter appears at the indicated position on the larger wheel. Then the handle is turned, which causes the encoder wheel to rotate, with the ciphertext appearing on the smaller wheel, as well as being printed on the paper tape. The cipher is its own inverse, so the decryption process is cryptographically identical to encryption.

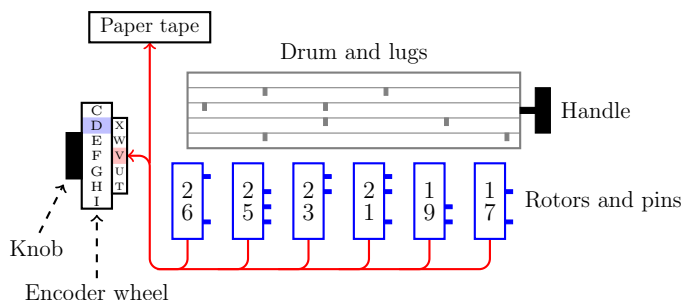


Figure 4: M-209 cipher diagram

In effect, at each encryption (or decryption) step, M-209 generates a pseudo-random number in the range of 0 to 27, which determines the number of positions that the encoder wheel turns. The stepping is dependent on the settings of the pins on the rotors and the lugs on the rotating drum—each drum bar for which a lug contacts an active pin causes the encoder wheel to rotate one position. After the pseudo-random step has been determined, each rotor is rotated one position, exposing a new set of pins for the next letter encryption. The ciphertext (or plaintext) letters are printed on the paper tape, as well as being visible on the smaller rotating letter wheel [3].

As mentioned above, the M-209 cipher is self-inverse, yet there is a switch that is set to specify encryption or decryption. The difference between encryption and

decryption modes is that for the former, ciphertext letters are printed in blocks of five on the paper tape, while for the latter, the letter Z is rendered as word-space<sup>2</sup>. Also, note that since the rotor lengths are relatively prime, the period until the pin positions are certain to repeat is

$$26 \times 25 \times 23 \times 21 \times 19 \times 17 \approx 2^{26.6}.$$

### 2.1.3 Sigaba

The ECM Mark II cipher machine, better known as **Sigaba**, is pictured in Figure 5. **Sigaba** is a rotor-based cipher created by American cryptographers, and it was employed by the United States during World War II and well into the 1950s. The cipher has five cipher rotors, and separate banks of rotors that are used to determine the stepping of the cipher rotors. In effect, it is somewhat analogous to an **Enigma** cipher with the another **Enigma** machine used to determine the stepping of the cipher rotors. No successful attacks on **Sigaba** are known to have occurred during its service lifetime.

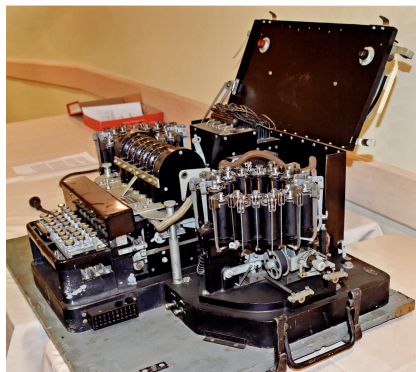


Figure 5: **Sigaba** cipher machine [1]

A diagram illustrating the cryptographically significant components of **Sigaba** is given in Figure 6. The cipher machine includes a keyboard for entering plaintext (or ciphertext) letters, an output device for printing the ciphertext (or plaintext), and fifteen rotors. Five cipher rotors are used to encrypt and decrypt, while the remaining ten rotors—five of which are referred to as control rotors and the remaining five are known as index rotors—control the stepping of the five cipher rotors. With each letter that is encrypted or decrypted, between one and four (inclusive) of the cipher rotors step. This highly irregular stepping results in a far more complex polyalphabetic substitution cipher, as compared to rotor machines that use a regular stepping motion; see [21] for more details on the inner workings of **Sigaba**.

---

<sup>2</sup>The M-209 manual states that each word-space is to be encrypted as Z. Thus, any plaintext Z will decrypt as a space on the paper tape, and hence when decrypting, Z would be inferred from context.

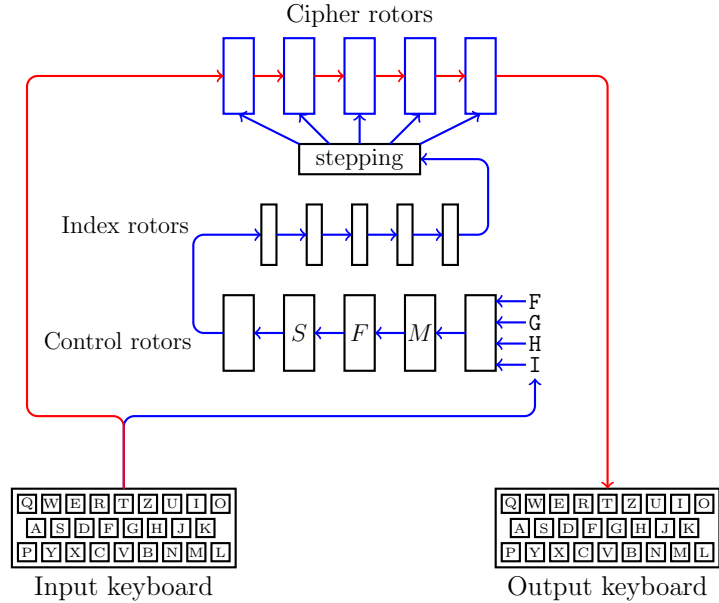


Figure 6: Sigaba cipher diagram

The cipher and control rotors are interchangeable and reversible, which greatly increases the number of combinations available. The index rotors serve to permute the numbers 0 through 9, and they do not step. The key consists of the order and orientation of the rotors and, of course, the initial position of each rotor can be adjusted.

### 2.1.4 Purple

The Japanese **Angooki Taipu B** cipher machine is better known by its nickname **Purple**, which is due to the binder color that United States cryptanalysts used to collect information on it. **Purple** was used for diplomatic communication during World War II, and it was used to encrypt the infamous “14-part message” that was sent from Tokyo to the Japanese embassy in Washington the day before the Japanese attack on Pearl Harbor.

No complete **Purple** cipher machine was ever found by the Allies although fragments were discovered after the war; Figure 7 shows one such fragment. Remarkably, American cryptographers were able to cryptanalyze the **Purple** cipher and regularly broke encrypted messages—including reading the “14-part message” before the Japanese embassy in Washington was able to decrypt it—in spite of never having seen the actual cipher machine. Perhaps even more remarkable, the **Purple** analog that the American cryptanalysts constructed used the same telephone selector switches that were in the actual Japanese **Purple** cipher.

The **Purple** cipher include an input plugboard, stepping switches, and an output plugboard [21]. Instead of using rotors to generate multiple alphabets,

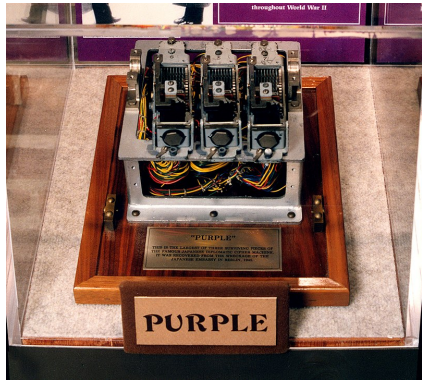


Figure 7: Fragment of Purple machine [17]

Purple has a number of hardwired permutations, where the aforementioned telephone selector switches are used to switch between the permutations. There are 25 permutations per switch, resulting in a hardware implementation that is far more complex than a rotor-based machine, with the switches resembling a rats nest of wires.

A diagram illustrating the cryptographic components of Purple is given in Figure 8. When a letter is typed on the input keyboard, it is passed through a plugboard, similar to the Enigma stecker, but including an unusual “6-20 split”, whereby 6 letters of the alphabet are treated differently than the other 20. If no cables are attached to the plugboard, the “sixes” are the vowels and the “twenties” are the consonants. In any case, letters among the sixes are encrypted via a single switch, and also serve to determine the stepping of the three switches that yield the twenties permutation.

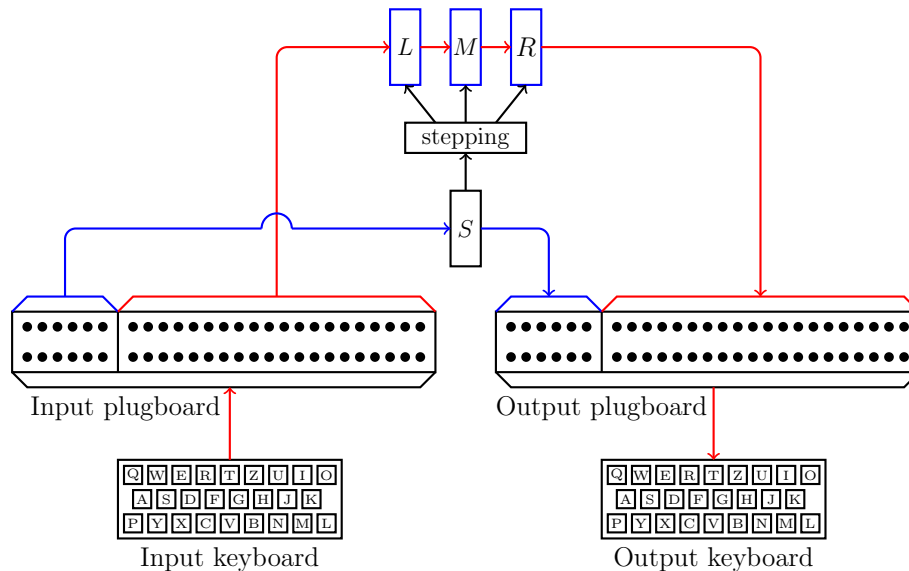


Figure 8: Purple cipher diagram



The 6-20 split is a major weakness of the **Purple** cipher, since the sixes have a different distribution from the twenties. We would expect that a machine learning algorithm will easily distinguish **Purple** ciphertext from the rotor-based ciphers that we consider and, in fact, we find that this is indeed the case.

### 2.1.5 **Typex**

**Typex**, originally known as “Enigma type with X-attachment”, is a rotor-based machine developed prior to WWII by O.G.W. Lywood for the British government [7]. As the original name implies, **Typex** was an adaptation of the commercial **Enigma**, with additional features designed to improve its security. There exist different variations of **Typex**, with a typical version having five rotors, a reflector, and a printer; later versions included an internal plugboard that was apparently used in place of the reflector [5]. A photo of a **Typex** machine appears in Figure 9.



Figure 9: **Typex** cipher machine [10]

A diagram illustrating the cryptographic components of **Typex** is given in Figure 10. Similar to the **Enigma** machine, when a letter is typed on the keyboard, it is sent through two stators, then the three stepping rotors, across the reflector, and back through the inverse of the same rotors and stators. Unlike **Enigma**, the medium and slow rotors of **Typex** step more than once per revolution their neighboring rotor. This irregular and more frequent stepping pattern makes attacks more challenging, as compared to **Enigma**.

## 2.2 Learning Algorithms

In this section we introduce the classic machine learning and deep learning algorithms that we use in our experiments. These are popular learning techniques that have been shown to perform well in a wide variety of applications.

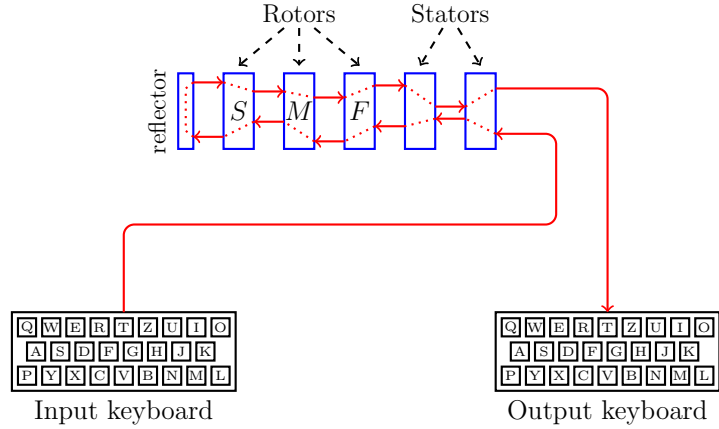


Figure 10: Typex cipher diagram

### 2.2.1 Support Vector Machine

Support Vector Machines (SVM) are one of the most popular supervised machine learning techniques for classification. The goal when training an SVM is to create a separating hyperplane where the margin, i.e., the minimum distance from the hyperplane to training samples, is maximized. However, this is not always possible to construct a separating hyperplane, as the data itself need not be linearly separable.

When training an SVM, the “kernel trick” enables us to map the data to a higher dimensional space, where separating the classes is generally easier [19]. In effect, the kernel trick allows us to embed a nonlinear transformation in the process, without paying a significant penalty, in terms of computational efficiency.

SVMs require a regularization hyperparameter  $C$  and, for nonlinear kernels,  $\gamma$ . The precise definition of  $\gamma$  depends on the specific nonlinear kernel function. The  $C$  parameter is related to the number of misclassifications that are allowed when constructing separating hyperplanes. The  $\gamma$  parameter can be viewed as defining how far the influence of each individual training sample extends. For our SVM experiments, we consider linear, Gaussian radial basis function (RBF), polynomial, and sigmoid kernel function.

### 2.2.2 $k$ -Nearest Neighbor

The  $k$ -Nearest Neighbor ( $k$ -NN) algorithm is a machine learning technique for classification that is based on the distance between feature values. The  $k$ -NN algorithm is said to be a “lazy learner,” since it requires no training—we simply classify a sample based on the  $k$  nearest samples in a specified training set. In spite of its simplicity, as the size of the training dataset grows,  $k$ -NN tends towards optimal, in a well-defined sense [19].

### 2.2.3 Random Forest

Random Forest (RF) classifiers are ensembles of decision trees. RF uses a “divide and conquer” approach to sample small subsets of the data and feature, with a decision tree constructed for each such subset. The RF classification is based on the combined predictions of its component decision trees [2]. Important hyperparameters in an RF include the number of estimators (i.e., decision trees), maximum features (maximum number of features to sample in any one decision tree), maximum depth of the decision trees, and “criterion” used to determine feature importance.

### 2.2.4 Multilayer Perceptron

The first of our deep learning algorithms in the Multilayer Perceptron (MLP), which is sometimes known simply as an Artificial Neural Network (ANN) that consists of multiple layers of perceptrons. A perceptron is a mathematical abstraction of a neuron [14]. An MLP is a feedforward technique that consists of at least three layers: the input layer, one or more hidden layers, and an output layer.

Important design decisions for MLPs include the depth, that is, the number of hidden layers, the number of neurons per layer, the activation functions, and the objective function. The objective function is minimized to train the corresponding MLP [18].

### 2.2.5 Long Short-Term Memory

Long Short-Term Memory (LSTM) networks are a class of Recurrent Neural Networks (RNNs) architecture. They can learn order dependencies in sequence prediction problems and are good at recognizing patterns in sequential data. RNNs, unlike other feedforward neural networks, have internal states that hold the context information about the previous inputs. Thus, the prediction at the current time step is dependent upon the context information from the previous time step. Plain “vanilla” RNNs struggle learning long term dependencies due to vanishing, exploding, or oscillating gradients that occur during training, which limits their memory capacity. LSTMs mitigate gradient issues, allowing for larger time lags from when a feature is introduced to the time at which it is used by the model. Thus, LSTMs can utilize past information more effectively than generic RNN models [19].

### 2.2.6 Extreme Learning Machines

An Extreme Learning Machine (ELM) is a feedforward deep learning algorithm with a simple architecture. Typically, ELMs have an input layer, a single hidden layer, and an output layer, with the number of neurons at the hidden layer being a configurable hyperparameter [19]. In an ELM, the hidden layer weights and biases are randomly assigned and are not updated via training—only the output

layer weights are trained, which can be accomplished using a linear algebraic techniques. Thus, there is no need for the costly backpropagation algorithm that is used to train most other neural networking architectures. Consequently, ELMs are extremely efficient to train, although they typically require more neurons than a comparable non-ELM architecture, which can make them slightly less efficient for classification [11].

### 2.2.7 Convolutional Neural Network

A Convolutional Neural Network (CNN) is a deep learning model that is designed to efficiently deal with image classification. For images, fully-connected neural networking architectures are too costly to train, and they tend to overfit the training data. CNNs are able to learn local dependencies, and they allow for a high degree of translation invariance [19]. Unlike other neural networking classification techniques, CNNs learn convolutional filters. CNN models typically consist of an input layer, multiple convolutional layers, pooling layers, and a fully-connected output layer. The first convolutional layer is applied to the input data, and enables the model to learn basic structures (e.g., edges), while each subsequent convolutional layer is applied to the output of the previous layer, resulting in convolutions of convolutions, which enables models to learn ever more abstract features. Pooling layers are used to reduce the dimensionality and increase translation independence. Many advanced CNN models have been pre-trained on vast image datasets—by retraining only the output layer, such model can be successfully applied to problem domains that are far different than the data on which they were originally trained.

## 3 Dataset and Experimental Design

This section details our dataset preparation and the design of our experiments. All models are developed in Python and use the `Scikit-learn` library. From the `Scikit-learn` library, the classification and metrics modules are used to evaluate the precision, recall, F1-score, and accuracy of the classifiers.

### 3.1 Dataset

To generate the data required to classify these ciphers, CrypTool-2, an application for cryptography and cryptanalysis, provided by the CrypToolProject has been used [12]. CrypTool-2 is an open source library that can be used to visualize, encrypt, and simulate most of the well-known Word War II era cipher machines, along with many other ciphers. To generate each ciphertext message, plaintext from the Brown Corpus is used [8]. The plaintext consists of 26 English alphabetic characters with no spaces, punctuation, or numbers. For each scenario, we use a balanced dataset of 1000 ciphertexts, each consisting of 1000 characters, which gives us 1,000,000 characters of ciphertext for each cipher.

Since we consider five ciphers, we have a total of 5000 samples and 5,000,000 ciphertext characters.

## 3.2 Feature Collection and Extraction

Features play an important role in training any learning model. We consider three different features, which are described in this section.

### 3.2.1 Histogram

For our first set of experiments, we consider histograms based on monograph statistics. That is, we simply count the frequency of each character per ciphertext message and normalize by the number of characters. Figure 11 shows the frequency per character from one **Enigma** ciphertext sample and its corresponding plaintext. Since **Enigma** is a polyalphabetic substitution cipher [21], the plaintext letters are enciphered differently based upon their position in the text and hence they have a more uniform distribution, as compared to the plaintext.

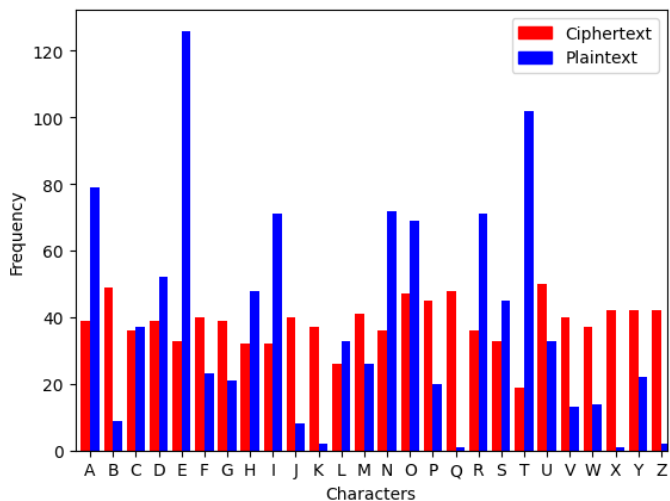


Figure 11: Histogram example

Figure 12 shows the relationship between the first five letters of the alphabet that appear in ciphertext for each of the ciphers that we consider. We observe that the **Purple** cipher clearly stands out from the rotor machines—especially with respect to the vowels—which is not surprising, given the 6-20 split of alphabet used by **Purple**. These graphs indicate that the **Purple** cipher will be easy to distinguish from the rotor cipher machines, but **Enigma**, **M-209**, **Sigaba**, and **Typex** from each other may be far more challenging.

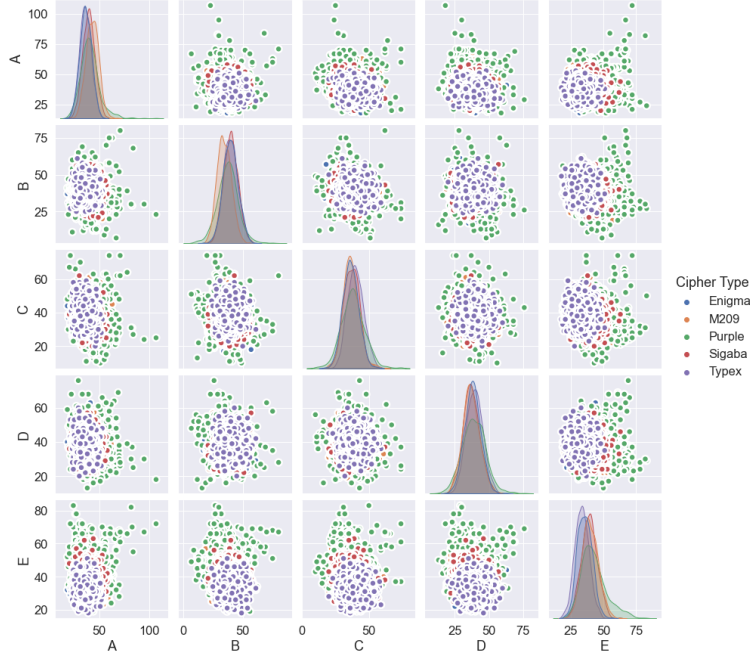


Figure 12: Character, cipher, and frequency relationship

### 3.2.2 Digram

Frequency analysis can be extended to multiple characters, not just monograph statistics. In general,  $n$ -gram sequences consist of  $n$  consecutive characters. In addition to the  $n = 1$  case discussed above, we consider the  $n = 2$  case, that is, digraphs or digrams. Digram counts are analogous to single character counts, but instead of counting the occurrences of every character, we count the frequency of pairs of characters. Note that this can be viewed as a feature vector of length  $26^2 = 676$ .

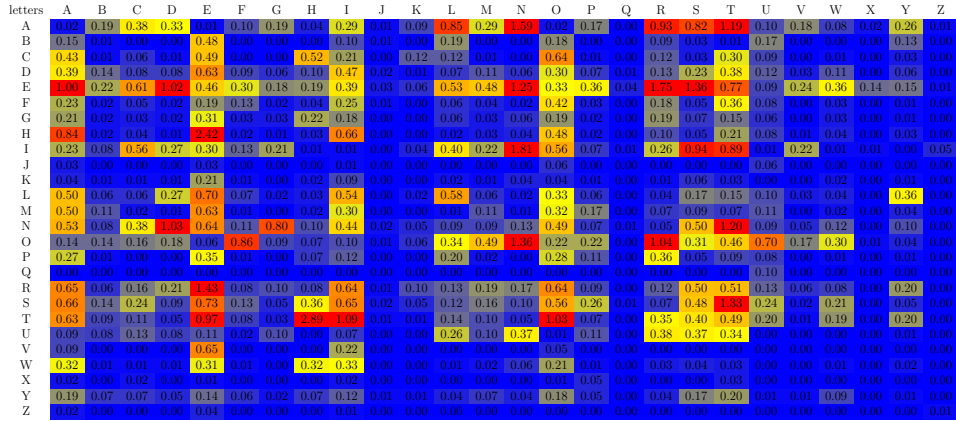
Figures 13(a) and (b) show heatmaps of digram letter frequencies for English text and **Enigma** ciphertext, respectively. We observe that the **Enigma** ciphertext has damped some of the roughness that is inherent in the plaintext, but it is still far from uniform.

### 3.2.3 Letter Sequence

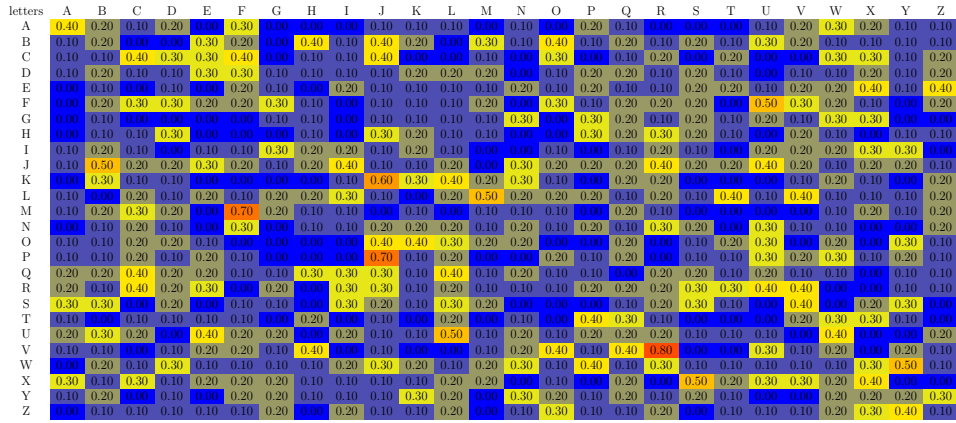
For our final set of classification experiments, we use the raw ciphertext letter sequences as our feature vectors. Since each ciphertext sequence is of length 1000, this gives us feature vectors of length 1000.

## 3.3 Overview of Experiments

Recall that for each of the five ciphers under consideration, we generate 1000 ciphertext messages, each of length 1000. Once all of the ciphertexts have been



(a) English plaintext



### 3.3.2 Random Plaintext and Fixed Keys

For this scenario, we use a different plaintext for each encryption, and again use a single fixed key for each cipher type. Otherwise, the processing of the data and generation of models is the same as in the fixed-fixed scenario. We refer to this as the “random-fixed” scenario.

### 3.3.3 Fixed Plaintext and Random Keys

Here, we use fixed plaintext, as in the fixed-fixed scenario, but for each encryption, we use a random key. Again, the processing of the data and generation of models is the same as in the fixed-fixed scenario. We refer to this as the “fixed-random” scenario.

### 3.3.4 Random Plaintext and Random Keys

For our final scenario, we use a random plaintext and a random key for each encryption. The processing of the data and generation of models is the same as in the fixed-fixed scenario discussed above. We refer to this as the “random-random” scenario.

Note that this random-random scenario is the most realistic. Hence, in the next section, we discuss our random-random experiments in detail, while most of the results involving the other three scenarios are relegated to the Appendix.

## 4 Random-Random Scenario Experiments

Since the random-random scenario is the most realistic, we provide a detailed discussion of our experiments and results for this case. Our experimental results for each of the other three scenarios is summarized in the Appendix.

For each of the three type of features considered, we generate seven models. Each of these 21 model is trained and tested using an 80-20 split, that is, 80% of the data is used for training, while the remaining 20% of the data is used for testing.

To measure and compare the quality of our results, for each experiment we compute the accuracy, precision, recall, and F1-score. Since there are 5000 samples for each experiment, and we use an 80-20 split, the total number of samples used for testing, or the support, is 1000. Also, since we use a balanced split, the support for each cipher is 200.

For each model, a grid search is used to tune the hyperparameters over reasonable sets of values. Table 1 lists the hyperparameters tested—as well as the hyperparameters selected—for each model when trained using each of the three feature types considered.



Table 1: Hyperparameters tested and selected

Learning technique	Hyperparameter	Tested	Selected		
			Histogram	Digram	Sequence
SVM	$C$	1, 10, 100, 1000	100	1	1
	$\gamma$	0.001, 0.0001	0.001	0.001	0.0001
	kernel	linear, poly, rbf, sigmoid	rbf	rbf	rbf
$k$ -NN	Number of neighbors	(1,2,...,200)	83	98	74
	Distance metric	Euclidean, manhattan, minkowski	Euclidean	Euclidean	manhattan
	Weights	uniform, distance	uniform	uniform	uniform
RF	Number of estimators	(1,2,...,200)	192	197	177
	Max depth	4, 5, 6, 7, 8	8	8	8
	Criterion	gini, entropy	gini	gini	gini
MLP	Activation function	tanh, relu	relu	relu	tanh
	$\alpha$	0.0001, 0.05	0.0001	0.0001	0.0001
	Hidden layer size	(100,200,15), (150,100,50), (500,)	(500,)	(500,)	(500,)
	Max iterations	200, 500, 1000	200	200	200
	Solver	sgd, adam	adam	adam	adam
ELM	Activation function	relu, sigmoid, tanh	relu	tanh	tanh
	Hidden neurons	(1,2,...,1000)	133	9696	995
LSTM	Number of hidden layers	1, 2, 3	3	2	2
	Activation function	relu, tanh, softmax	softmax	softmax	softmax
	Dropout rate	0.1, 0.3, 0.9	0.3	0.3	0.3
CNN	Number of layers	3, 4, 5	5	5	5
	Activation function	sigmoid, softmax	sigmoid	sigmoid	sigmoid
	Dropout rate	0.1, 0.3, 0.5	0.3	0.3	0.3

## 4.1 Histogram Experiments

In this section, we test each of the seven models discussed in Section 2 using the histogram features. Note that the histogram feature vector is of length 26 for each sample. We provide a few relevant additional details on the training of each of the models. Finally, after discussing the models, we summarize the results for each.

When training our SVM models, we must determine the hyperparameter  $\gamma$ , the regularization parameter  $C$ , and the kernel function. For the kernel function, we consider linear, polynomial, radial basis function, and sigmoid, and we test reasonable values for  $\gamma$  and  $C$ . For the histogram features, we find that the sigmoid kernel yields the best results.

For  $k$ -NN, we must first determine the value of  $k$ , which is the number of nearest neighbors considered when classifying a sample. In general, setting  $k$  too small results in overfitting, while too large of a value can cause underfitting. From the results in Figure 14, we determine that the optimal value is  $k = 83$ .

Another  $k$ -NN hyperparameter that we experimented with is selecting the best distance metric between neighbors. There are many different distance formulas available but we tested the most popular to reduce the hyperparameter grid computations. We also test whether the model does better when all points in each neighborhood are weighted equally or if they are weighted, based on their distance from the sample being classified.

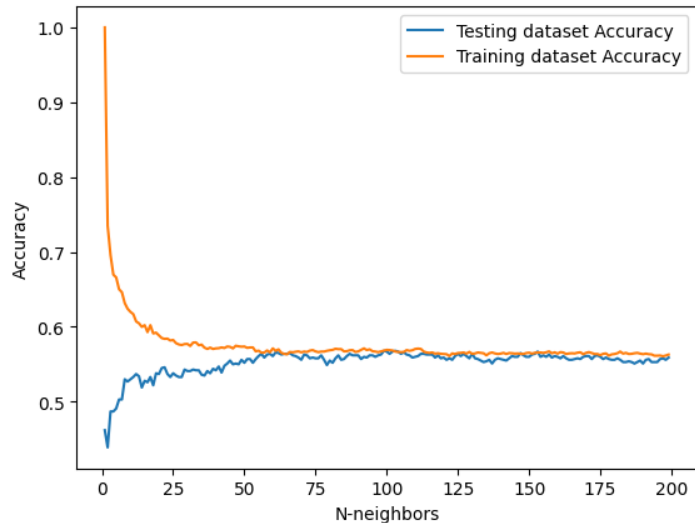


Figure 14: Histogram  $k$ -NN number of neighbors and accuracy

For our Random Forest classifier, we experiment with the so-called number of “estimators”, that is, the number of decision trees used. We use “sqrt” for our maximum number of features, that is, the square root of the total number of features in the dataset [16]. The maximum depth, which represents the longest path between the root node and the leaf node, was tested as part of our grid search.

For our MLP, we test a wide range of hyperparameters. Specifically, our grid search includes the activation function, the regularization term, the size of the hidden layers, the maximum number iterations, and the weight optimization (or solver).

For our ELM, we experiment with the number of neurons in the hidden layer, and activation functions. It is important to change the encoding of our target variables with ELM, since the classification only works with discrete classes. We transform the single values of the target variable into a vector via one-hot encoding as given in Table 2.

Table 2: One-hot encodings

Enigma	(1, 0, 0, 0, 0)
M-209	(0, 1, 0, 0, 0)
Purple	(0, 0, 1, 0, 0)
Sigaba	(0, 0, 0, 1, 0)
Typex	(0, 0, 0, 0, 1)

From Figure 15, we see that the accuracy of our ELM plateaus after about 50 hidden neurons. However, the maximum accuracy is attained with 133 neurons, so that is what we use for this model.

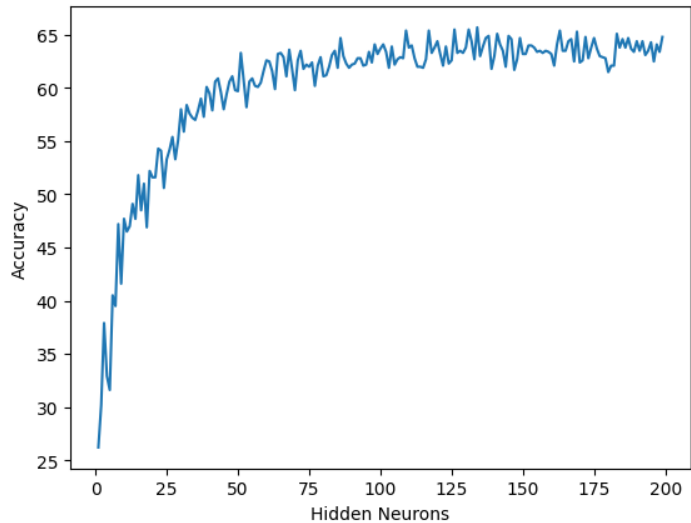


Figure 15: Histogram ELM accuracy and number of hidden neurons

For our LSTM architecture, we experiment with the number of hidden layers, the activation function, and the dropout rate. A basic LSTM architecture includes an input layer, a single hidden layer, and an output layer. There are no clear guidelines on how to determine the number of layers for an LSTM, although [22] notes that, theoretically, one hidden layer often works well, and two layers are typically enough to learn more complex problems. For the histogram features we found that two sequential layers, a dropout layer, and an output layer produce the best result. From the loss and accuracy graphs in Figure 16, we see the result of training for 15 epochs, and we note that there is no indication of overfitting in these graphs.

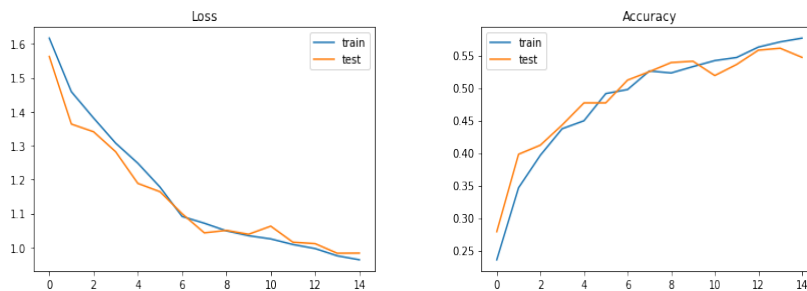


Figure 16: Loss and accuracy of histogram LSTM model

We train a two-dimensional CNN. To create the “images” needed for training such a CNN, we use a heatmap of the histogram statistics. For our CNN architecture, we experiment with the number of convolutional layers, the activation function, and the dropout rate. For the histogram data we found that a CNN with three convolutional layers yields the best results.

Based on the loss and accuracy graphs in Figure 17, we observe that after training for 32 epochs, the loss is about 1.07 and the accuracy is only about 0.49. We again see no evidence of overfitting in these graphs.

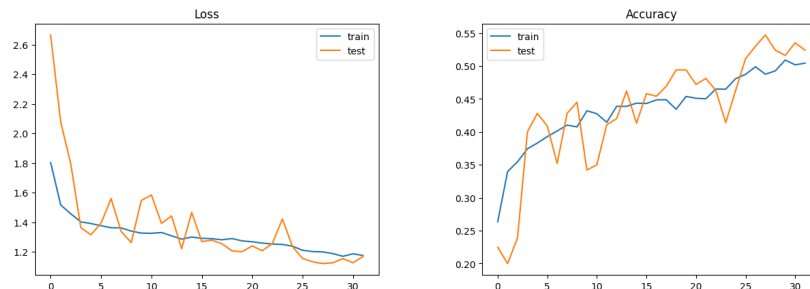


Figure 17: Loss and accuracy of histogram CNN model

Precision, recall, and F1-scores for each cipher and each learning technique—when trained on the histogram features as discussed above—are given in the bar graphs in Figure 18. We note that for this case, M-209 is easily distinguished from the rotor-based ciphers, while the most similar ciphers—Enigma, Sigaba, and Typex—are not accurately distinguished.

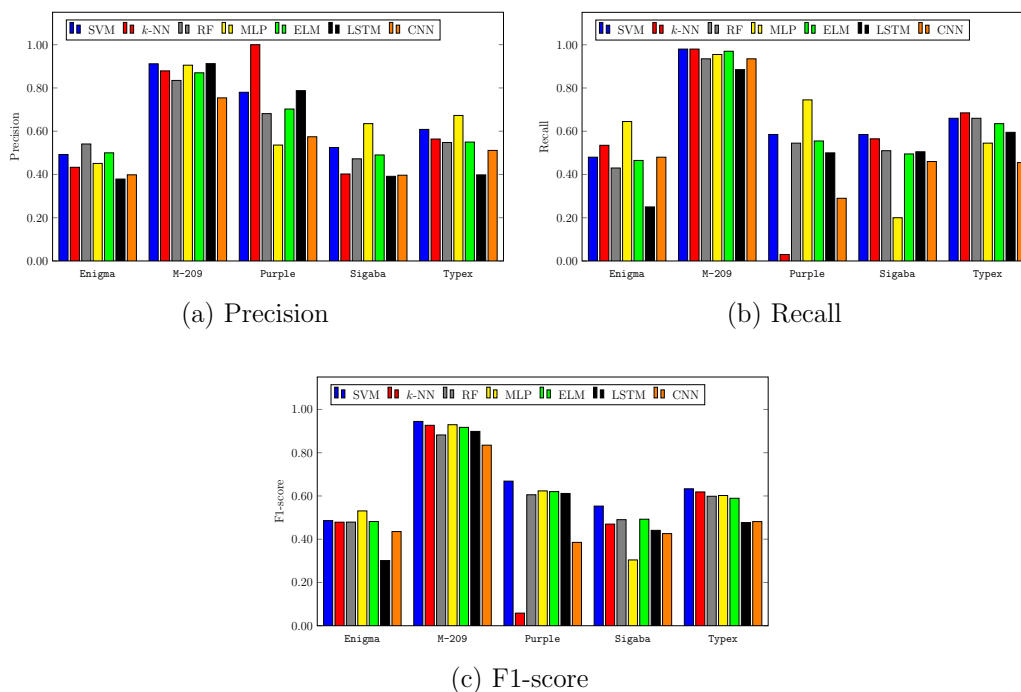


Figure 18: Precision, recall, and F1-scores for histogram features

A confusion matrix for each of the experiments in this section is given in the Appendix in Figure 23. We observe that Typex and Enigma are the most often

confused with each other. This is not surprising, given that **Typex** is a variant of the commercial version of **Engima**.

## 4.2 Digram Experiments

Training models using the digram features follows a similar pattern as discussed above for the histogram features. and hence we omit the details. As for the histogram features, we found no evidence of overfitting for the models when using the digram features. Recall that the hyperparameters selected in this case are given in the penultimate column of Table 1.

The results of our digram experiments are summarized in Figure 19. We note that the results are similar to those obtained for the histogram features, above.

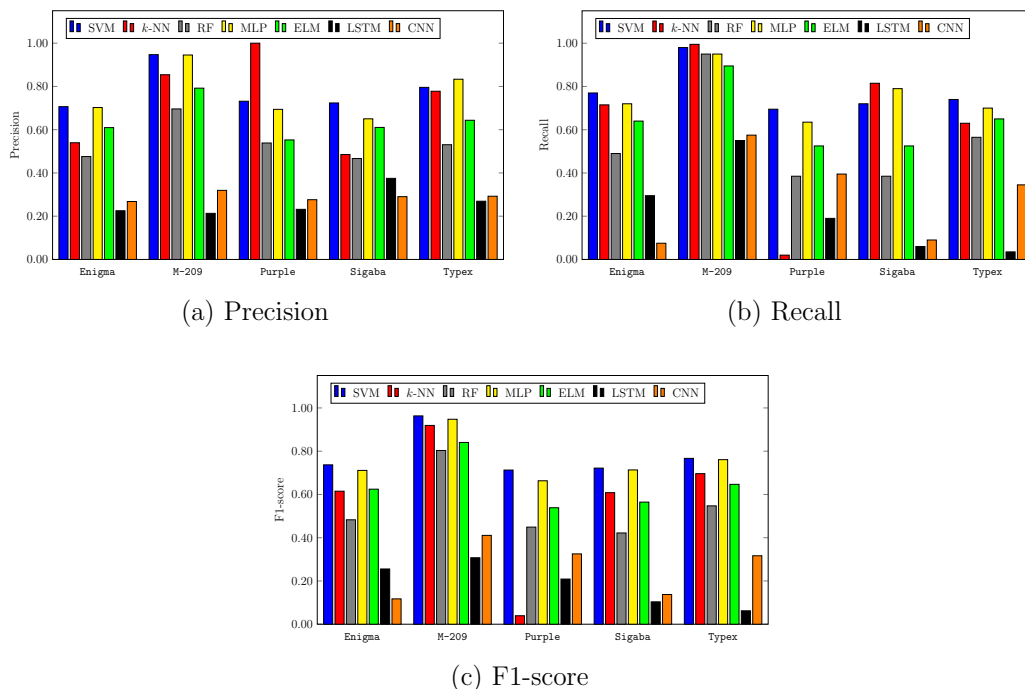


Figure 19: Precision, recall, and F1-scores for digram features

Confusion matrices for all of the digram experiments in this section are given in the Appendix in Figure 24.

## 4.3 Letter Sequence Experiments

Our models trained using letter sequence features again follow a similar pattern as for the histogram and digram features, so we omit the details. We again found no evidence of overfitting for the models when using the letter sequence features. The hyperparameters selected in this case are given in final column in Table 1.

The results of our letter sequence experiments are summarized in Figure 20. We note that the best of these results are clearly much stronger than those obtained for the histogram or digram features, above.

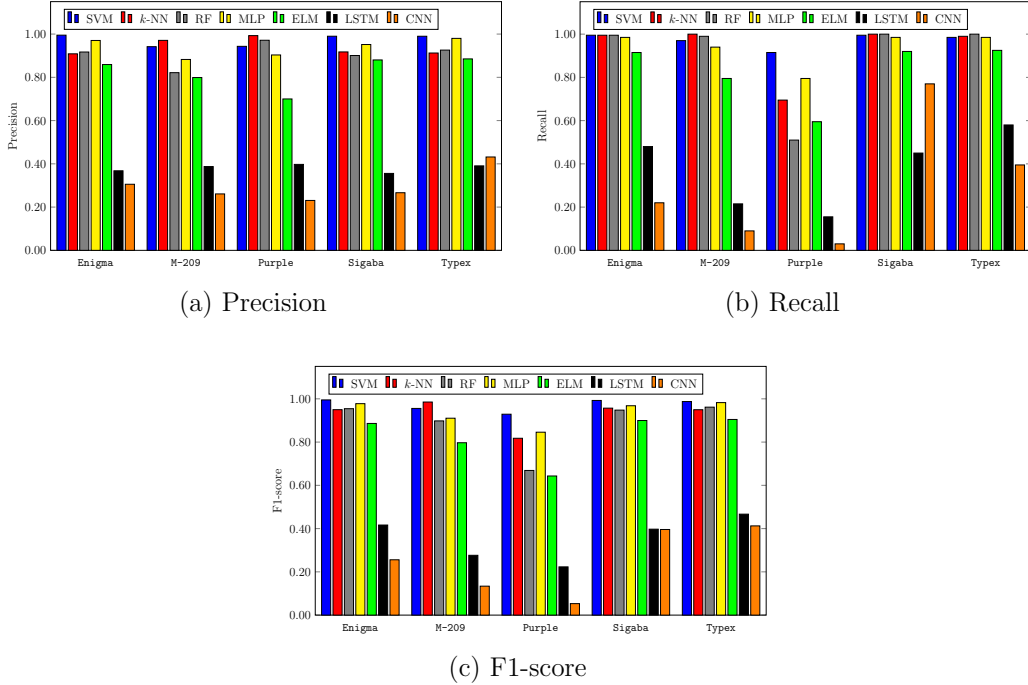


Figure 20: Precision, recall, and F1-scores for letter sequence features

Confusion matrices for all of the digram experiments in this section are given in the Appendix in Figure 25.

## 4.4 Reduced Ciphertext Length

All of the experiments above are based on ciphertext messages of length 1000. In this section, we consider the effect on classification accuracy when less ciphertext is available. Since the random-random case is the most realistic, and since SVM and MLP models with letter sequence and diagram features performed best, this scenario with these models and features are considered here.

In Figure 21(a), we give results for both the SVM and MLP models, based on the digram features. We observe that the SVM performs better for every length tested. Furthermore, for the SVM model, the accuracy drops from 0.781 for ciphertext of length 1000 to 0.685 for ciphertext of length 300, and the model achieves a respectable accuracy of 0.527 with just 50 ciphertext characters.

Note that for the digram feature, regardless of the ciphertext length, the feature vector is of length  $26^2 = 676$ . Hence, we can—and do—use the models trained on 1000 ciphertext symbols to test each ciphertext length.

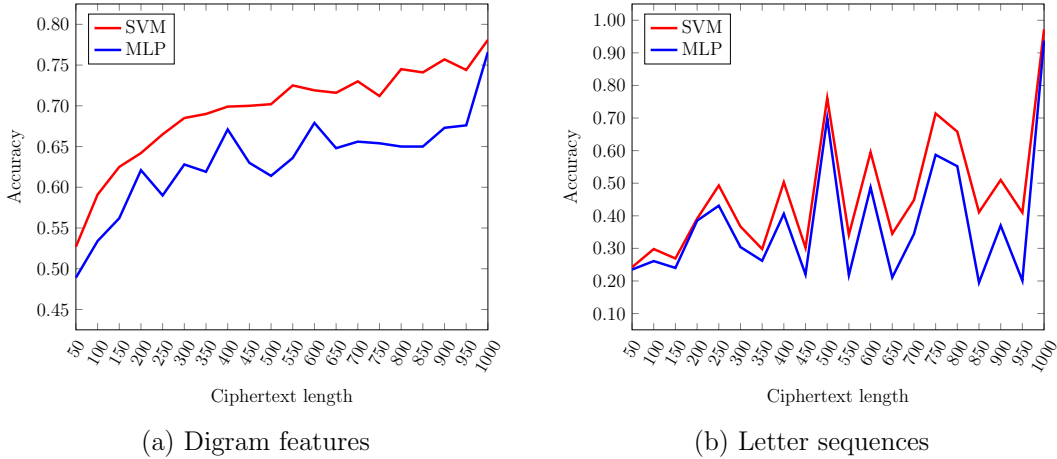


Figure 21: Accuracy as a function of ciphertext length

In Figure 21(b), we give results for both the SVM and MLP models, based on the ciphertext letter sequences. In this case, the results are wildly inconsistent; for example, the MLP drops from an accuracy of 0.938 with ciphertext of length 1000 to an accuracy that is no better than guessing (0.201, to be precise) for length 950, and then rebounds to an accuracy of 0.699 at length 500.

For each different ciphertext length, the models in Figure 21(b) must be retrained, as the feature vector length has changed. Due to time constraints, we did not tune the hyperparameters when retraining the models, but instead used the optimal hyperparameters for the length 1000 models. Consequently, the unstable results in Figure 21(b) indicate that these models are likely very sensitive to proper tuning of the hyperparameters, at least for the classic cipher classification problem considered in this paper.

## 4.5 Discussion

For our random-random scenario experiments, the overall accuracy for each of the seven models and each of the three feature types is given in Figure 22(a). The corresponding accuracies for the fixed-fixed, random-fixed, and fixed-random scenarios are given in Figures 22(b) through (d), respectively.

From the graphs in Figure 22, it is apparent that random keys are necessary for the models to accurately distinguish between the ciphers. Curiously, in the fixed key cases, the letter sequence feature performs particularly poorly, while it is the best feature in both of the random-key scenarios.

Classifying ciphertexts using machine learning is a challenging task, as any well-designed cipher should produce ciphertext that is close to “random.” Nevertheless, in our random-random scenario experiments, the best classification accuracy that we obtained was slightly more than 97% for an SVM model trained on ciphertext letter sequences, while MLP and  $k$ -NN models—also trained on letter sequences—were next best at 93.8% and 93.6% accuracy, respectively.

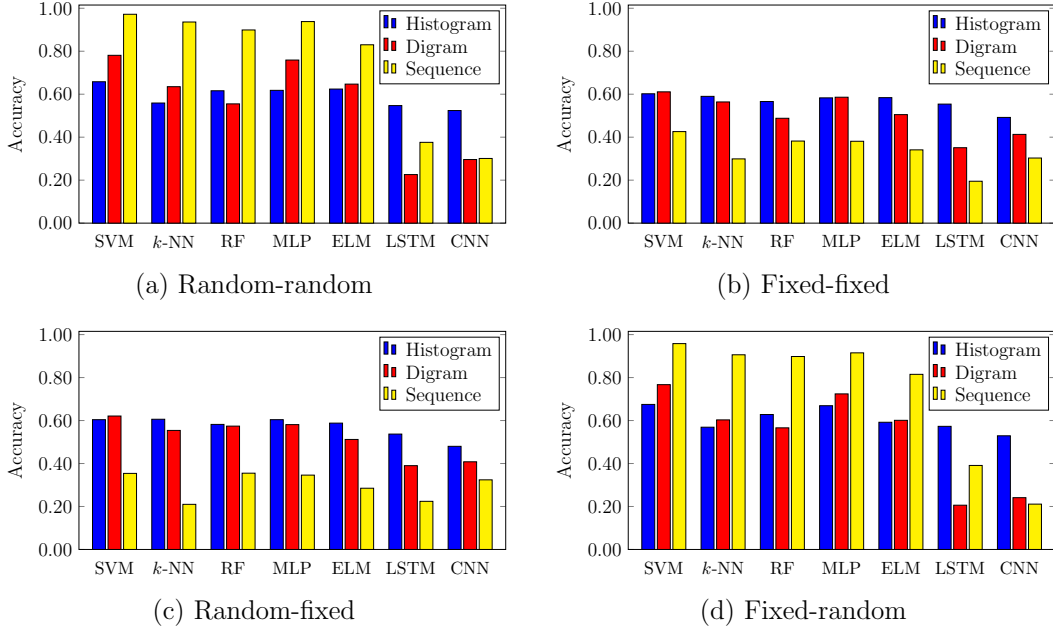


Figure 22: Model accuracies for each scenario

In contrast to the letter sequence feature, for the histogram feature, our best accuracy for the random-random scenario was only 66%, while for the digram feature, the best accuracy was 78%. For both of these feature types, the SVM was also the best model. In all scenarios, the LSTM and CNN models perform relatively poorly.

## 5 Conclusion and Future Work

For the five different WWII ciphers considered in this research, we have shown that machine learning algorithms can determine the cipher type from ciphertext only, with high accuracy. Our best results for the most realistic scenario (i.e., random plaintext and random keys) are summarized in Figure 22(a), above. Overall, the SVM performed best, with MLP and  $k$ -NN being next best.

We found that among the five cipher machines considered, M-209 was consistently the easiest cipher to classify, and Purple was generally relatively easy to distinguish. These results are not surprising, since the rotor system in M-209 is much different than that used in the other rotor-based ciphers considered, while the 6-20 split used by Purple should make its switch-based system stand out. The most challenging ciphers to distinguish between are Typex and Enigma which, again, is not surprising, since these ciphers share a common ancestor in the form of the original commercial Enigma machine. However, in spite of being the most challenging case, distinguishing between Typex and Enigma is fairly easy for our best models.



Future work could involve additional ciphers, additional learning techniques, ensemble techniques, further hyperparameter tuning, and consideration of additional features and feature engineering techniques. For example, our CNN results were not impressive, but using pre-trained models, such as VGG19 or any of the popular ResNet models would be well worth considering. Also, we expected the LSTM to perform well on the letter sequence features, yet the results for this model were consistently poor, perhaps due to insufficient training. This too is worth further study.

## References

- [1] Donald Aldridge. SIGABA photographic print. <https://5099.sydneyplus.com/final/ViewImage.aspx?template=Image&field=DerivedIma&hash=6992c5bb0cd84f7c8fe1ef6baa798f3f&r=1552548062&lang=en-US>.
- [2] Gérard Biau and Erwan Scornet. A random forest guided tour. *Test*, 25(2):197–227, 2016.
- [3] Mark J. Blair. Converter M-209-B. <https://www.nf6x.net/2009/02/converter-m-209-b/>, 2009.
- [4] Kenneth J. Bures. Cracking PURPLE: the identification of homologs in the cryptanalysis of the Angooki Taipu B cipher machine. *Cryptologia*, pages 1–13, 2022.
- [5] Kelly Chang, Richard M. Low, and Mark Stamp. Cryptanalysis of Typex. *Cryptologia*, 38(2):116–132, 2014.
- [6] The Enigma machine. <https://www.tnmoc.org/bh-2-the-enigma-machine>.
- [7] Ralph Erskine. The development of Typex. *The Enigma Bulletin*, 2:69–85, 1997.
- [8] W. Nelson Francis and Henry Kucera. Brown corpus manual. *Letters to the Editor*, 5(2), 1979.
- [9] James J. Gillogly. Ciphertext-only cryptanalysis of Enigma. *Cryptologia*, 19(4):405–413, 1995.
- [10] Martin Gillow. What was Typex? <https://typex.virtualcolossus.co.uk/typex.html>.
- [11] Guang-Bin Huang, Qin-Yu Zhu, and Chee-Kheong Siew. Extreme learning machine: Theory and applications. *Neurocomputing*, 70(1):489–501, 2006.
- [12] Nils Kopal. Solving classical ciphers with CrypTool 2. In *Proceedings of the 1st International Conference on Historical Cryptology*, HistoCrypt, pages 29–38, 2018.

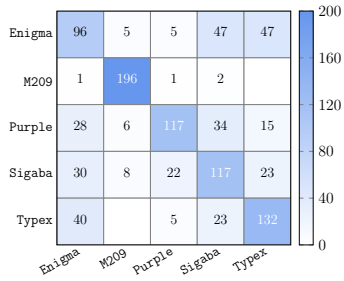
- [13] Nivedhitha Ramarathnam Krishna. Classifying classic ciphers using machine learning. Master’s thesis, Department of Computer Science, San José State University, 2019.
- [14] Pierre Lorrentz. *Artificial Neural Systems: Principle and Practice*. Bentham Science Publishers, 2015.
- [15] The cipher machine M-209. <http://www.jfbouch.fr/crypto/m209/index.html>.
- [16] F. Pedregosa et al. Scikit-learn: Machine learning in Python. *Journal of Machine Learning Research*, 12:2825–2830, 2011.
- [17] Japanese PURPLE cipher machine fragment. <https://5099.sydneyplus.com/final/ViewImage.aspx?template=Image&field=DerivedIma&hash=2a4749d2b7fdec86e7b1abf56550077c&width=max&height=max&r=1552548062&lang=en-US>.
- [18] Sebastian Ruder. An overview of gradient descent optimization algorithms. <https://arxiv.org/abs/1609.04747>, 2016.
- [19] Mark Stamp. *Introduction to Machine Learning with Applications in Information Security*. Chapman and Hall/CRC, second edition, 2022.
- [20] Mark Stamp and Wing On Chan. Sigaba: Cryptanalysis of the full keyspace. *Cryptologia*, 31(3):201–222, 2007.
- [21] Mark Stamp and Richard M. Low. *Applied Cryptanalysis: Breaking Ciphers in the Real World*. John Wiley & Sons, 2007.
- [22] Dimitris Stathakis. How many hidden layers and nodes? *International Journal of Remote Sensing*, 30(8):2133–2147, 2009.

## Appendix

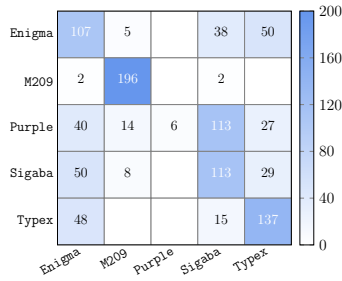
In this appendix, we provide confusion matrices for the random plaintext with random keys (random-random) scenario. In addition, we summarize the results for the other three scenarios considered, namely, the fixed plaintext with fixed keys (fixed-fixed), random plaintext with fixed keys (random-fixed), and fixed plaintext with random keys (fixed-random).

### Random-Random Scenario Confusion Matrices

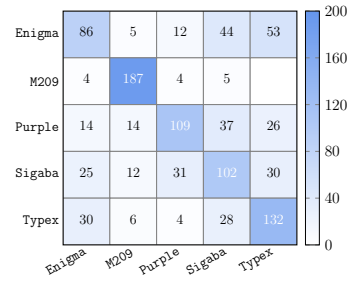
Here, we give confusion matrices for each of the random-random scenario experiments discussed in Section 4. Recall that we considered seven models (SVM,  $k$ -NN, RF, MLP, ELM, LSTM, and CNN) and three feature types (histogram, digram, and letter sequence), and hence we have a total of 21 confusion matrices. The confusion matrices for the histogram features are in Figure 23, while those for the digram features are in Figure 24, and the confusion matrices for the letter sequence features are in Figure 25.



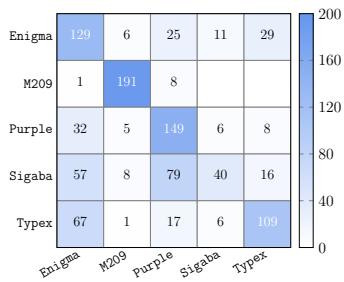
(a) SVM



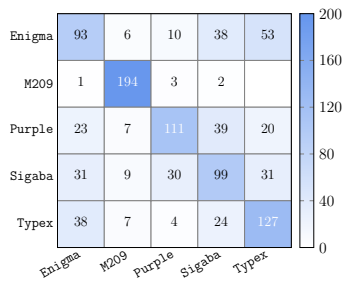
(b)  $k$ -NN



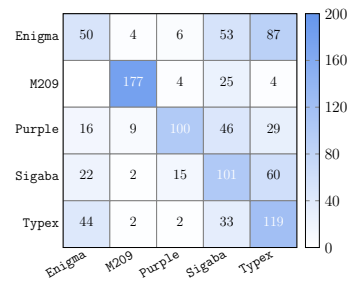
(c) RF



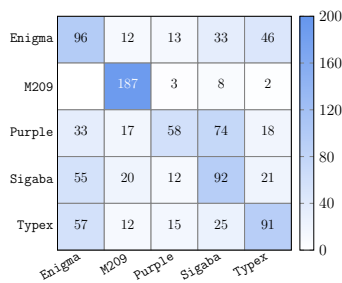
(d) MLP



(e) ELM

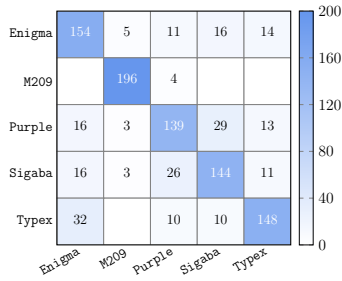


(f) LSTM

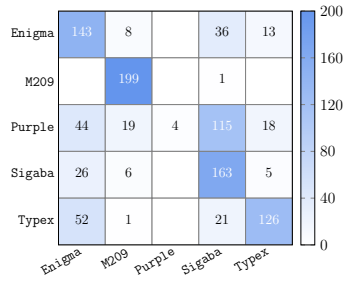


(g) CNN

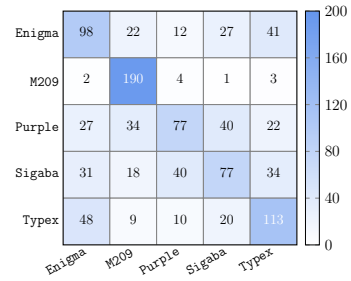
Figure 23: Random-random confusion matrices for histogram features



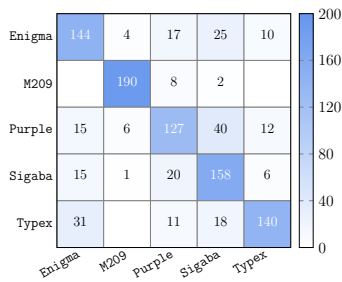
(a) SVM



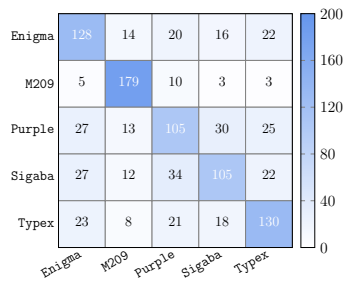
(b)  $k$ -NN



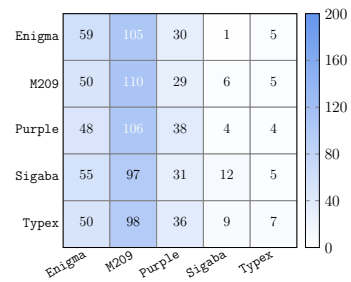
(c) RF



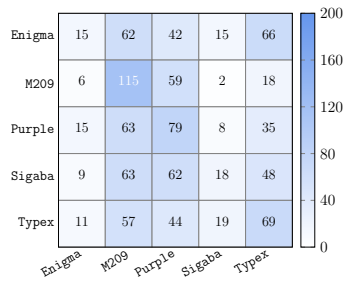
(d) MLP



(e) ELM



(f) LSTM



(g) CNN

Figure 24: Random-random confusion matrices for digram features

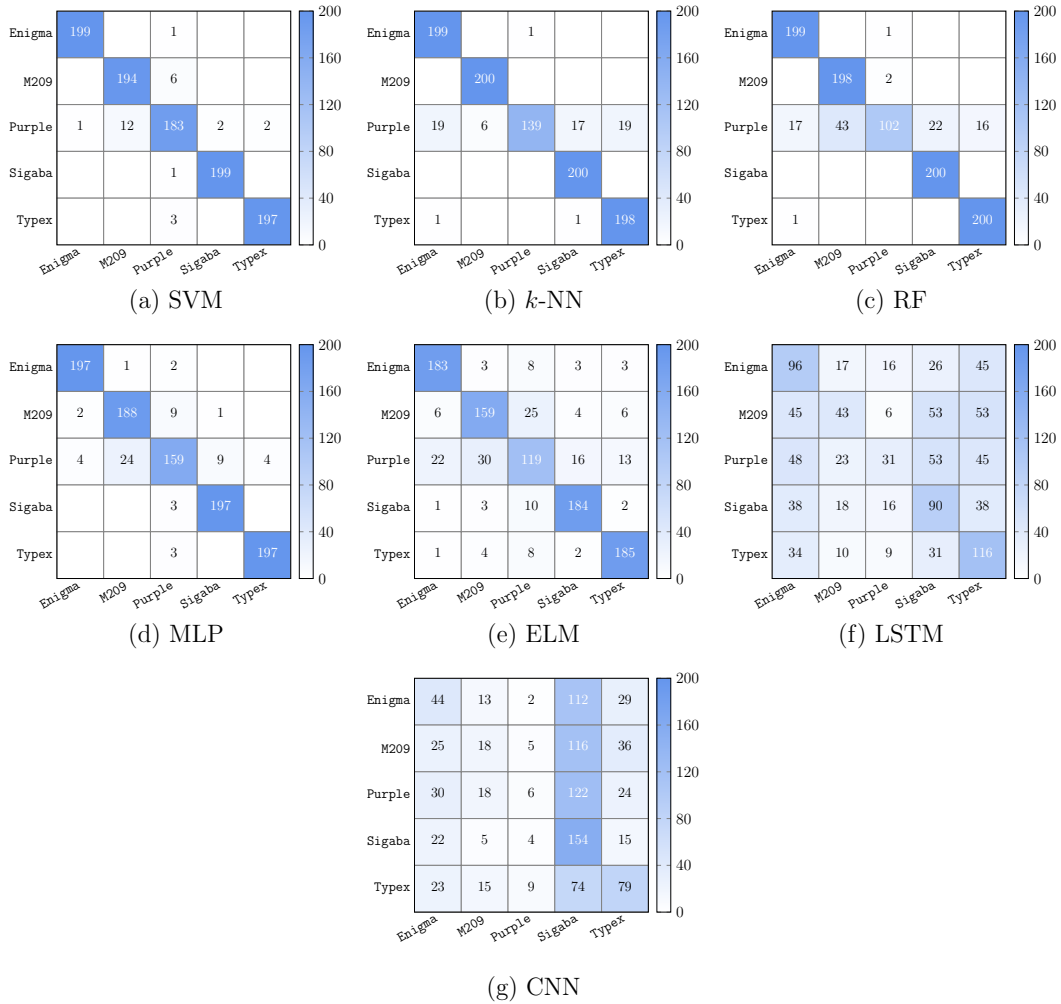


Figure 25: Random-random confusion matrices for letter sequence feature

## Summary of Results for Fixed-Fixed Scenario

In this section, we give results for the fixed-fixed scenario, which is discussed in Section 3.3.1. We experiment with each of the seven models (SVM,  $k$ -NN, RF, MLP, ELM, LSTM, and CNN) using each of the three feature types (histogram, digram, and letter sequence) for a total of 21 distinct models. For each model, we provide a confusion matrix, and we give the precision, recall, and F1-score for each of the five ciphers in bar graph form. The confusion matrices and bar graphs for the histogram features appear in Figures 26 and 27, respectively; the confusion matrices and bar graphs for the digram features are in Figures 28 and 29, respectively; and the confusion matrices and bar graphs for the letter sequence features are in Figures 30 and 31.

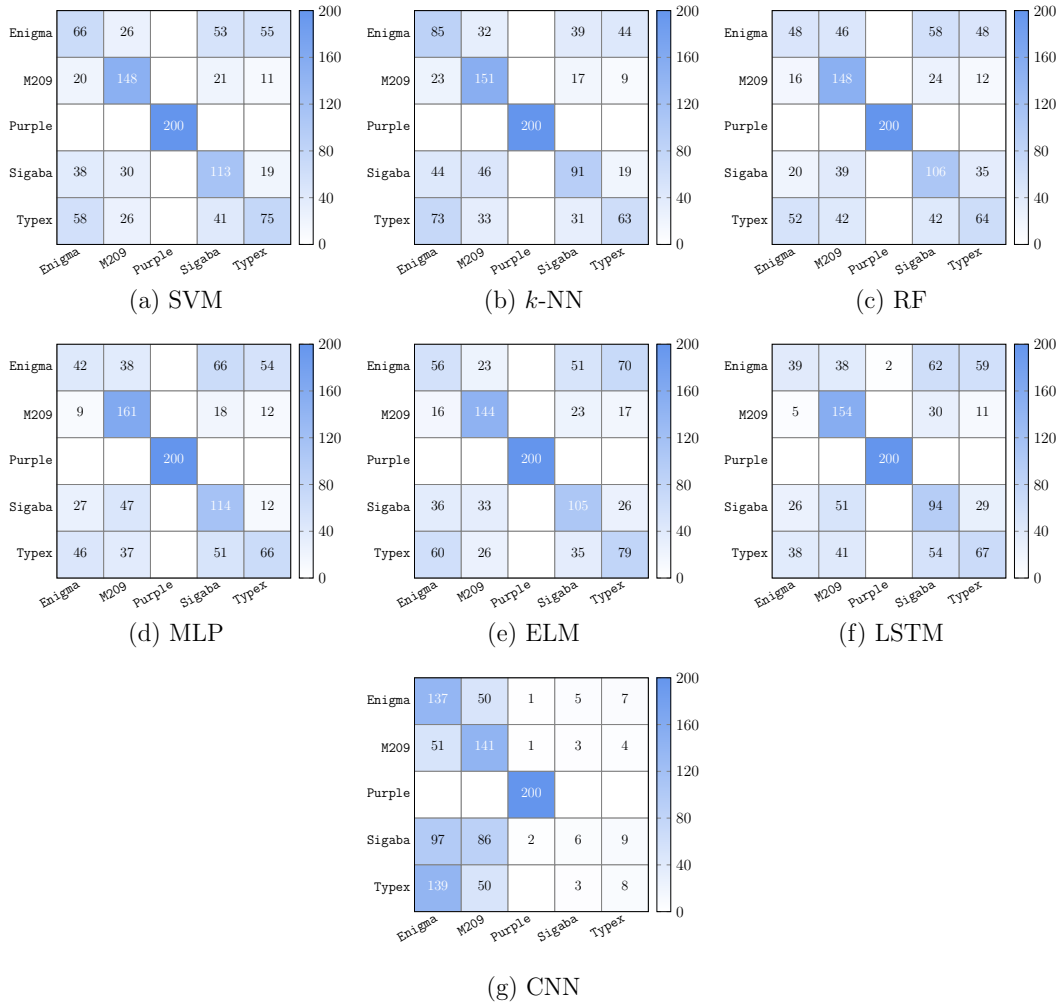


Figure 26: Fixed-fixed confusion matrices for histogram features

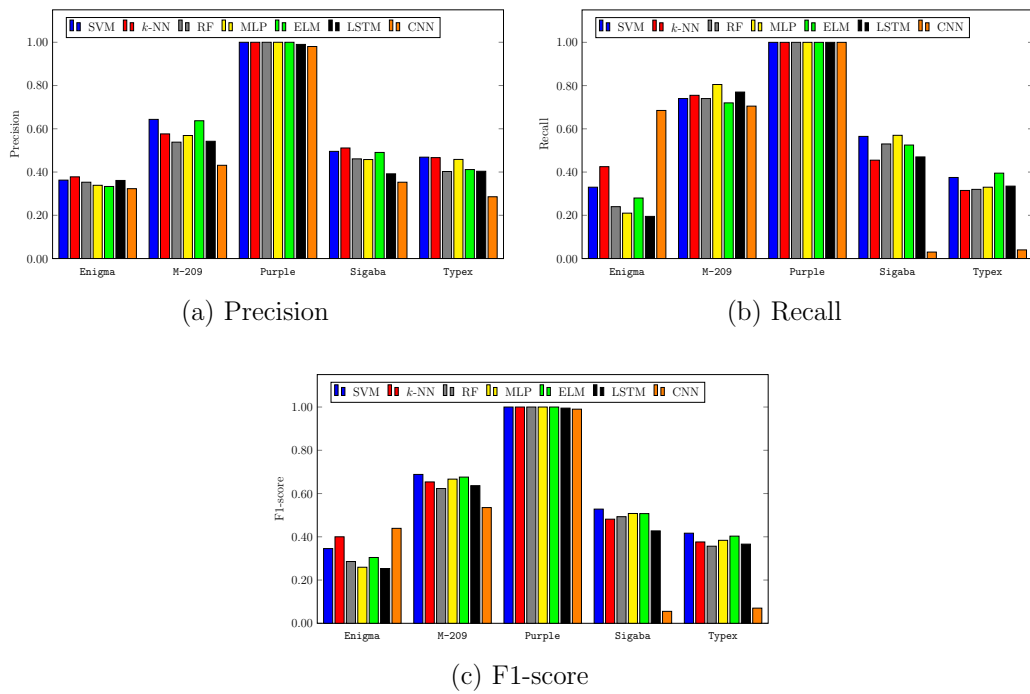
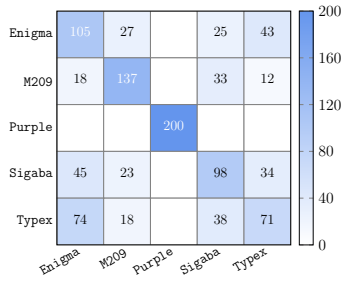
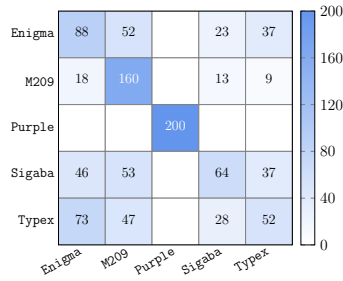


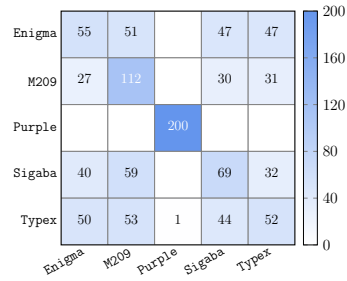
Figure 27: Fixed-fixed precision, recall, and F1-scores for histogram features



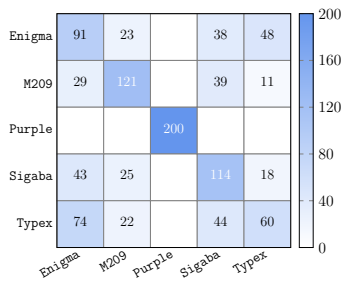
(a) SVM



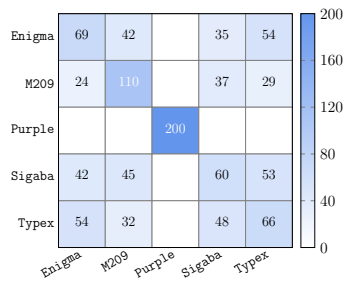
(b)  $k$ -NN



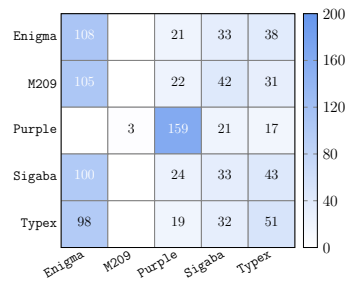
(c) RF



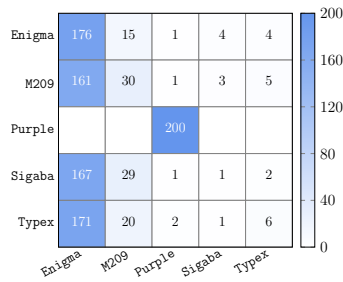
(d) MLP



(e) ELM



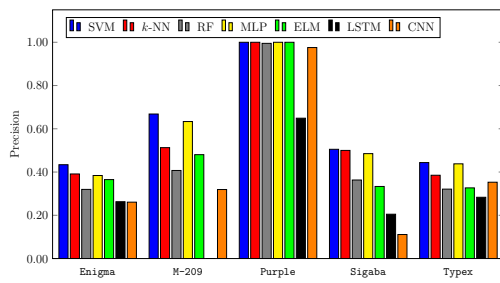
(f) LSTM



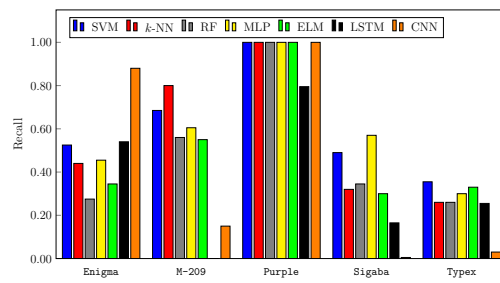
(g) CNN

Figure 28: Fixed-fixed confusion matrices for digram features

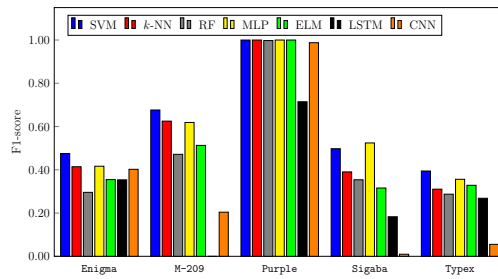




(a) Precision

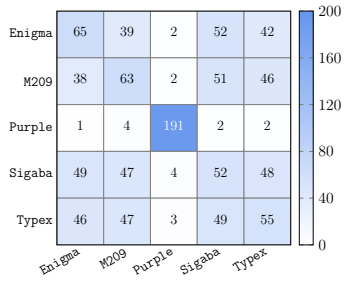


(b) Recall

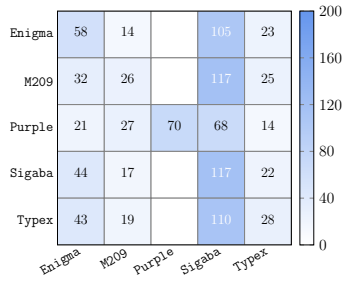


(c) F1-score

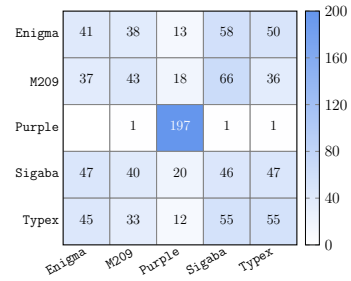
Figure 29: Fixed-fixed precision, recall, and F1-scores for digram features



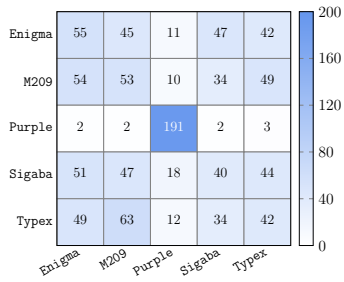
(a) SVM



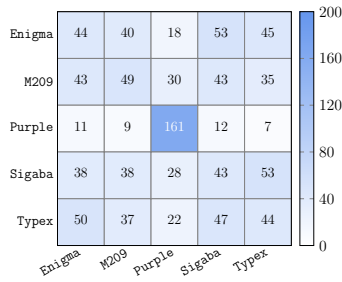
(b)  $k$ -NN



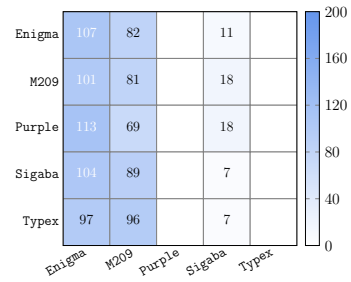
(c) RF



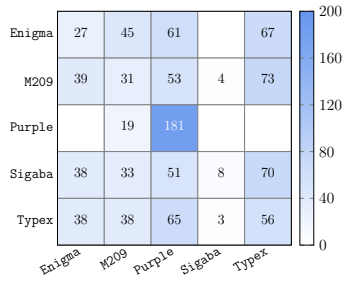
(d) MLP



(e) ELM



(f) LSTM



(g) CNN

Figure 30: Fixed-fixed confusion matrices for letter sequence feature

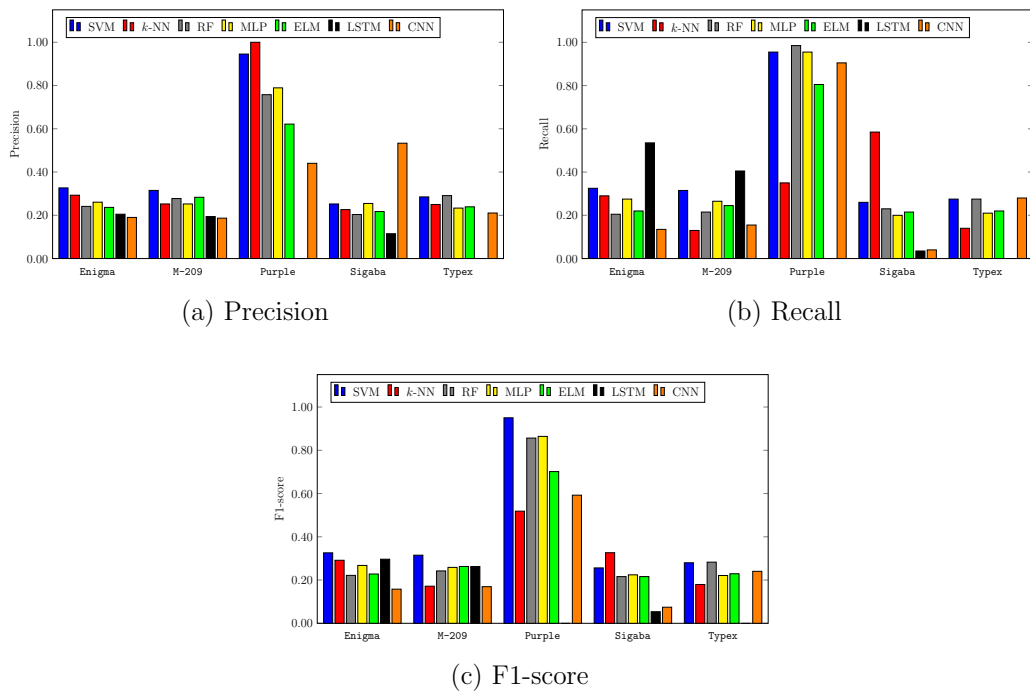


Figure 31: Fixed-fixed precision, recall, and F1-scores for letter sequence features

## Summary of Results for Random-Fixed Scenario

In this section, we give results for the random-fixed scenario, which is discussed in Section 3.3.2. We experiment with each of the seven models (SVM,  $k$ -NN, RF, MLP, ELM, LSTM, and CNN) using each of the three feature types (histogram, digram, and letter sequence) for a total of 21 distinct models. For each model, we provide a confusion matrix, and we give the precision, recall, and F1-score for each of the five ciphers in bar graph form. The confusion matrices and bar graphs for the histogram features appear in Figures 32 and 33, respectively; the confusion matrices and bar graphs for the digram features are in Figures 34 and 35, respectively; and the confusion matrices and bar graphs for the letter sequence features are in Figures 36 and 37.

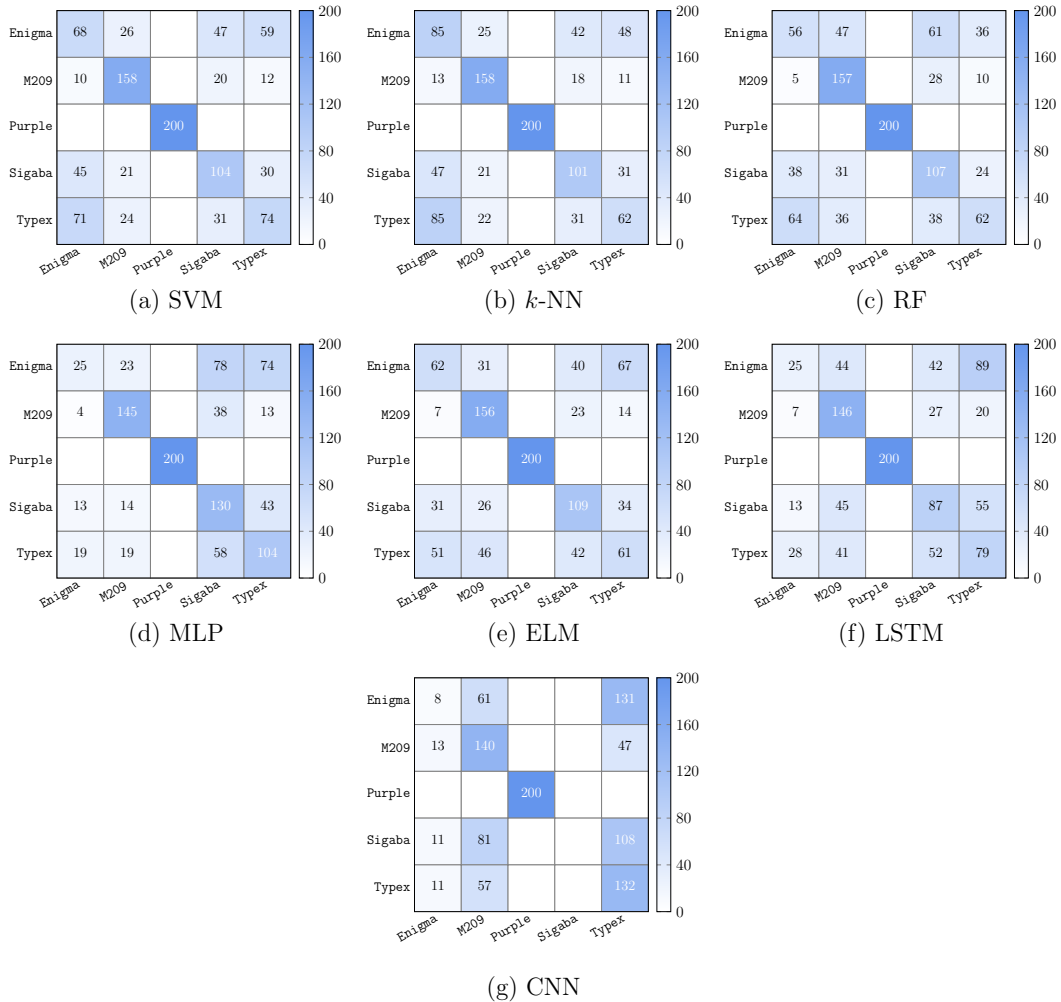


Figure 32: Random-fixed confusion matrices for histogram features

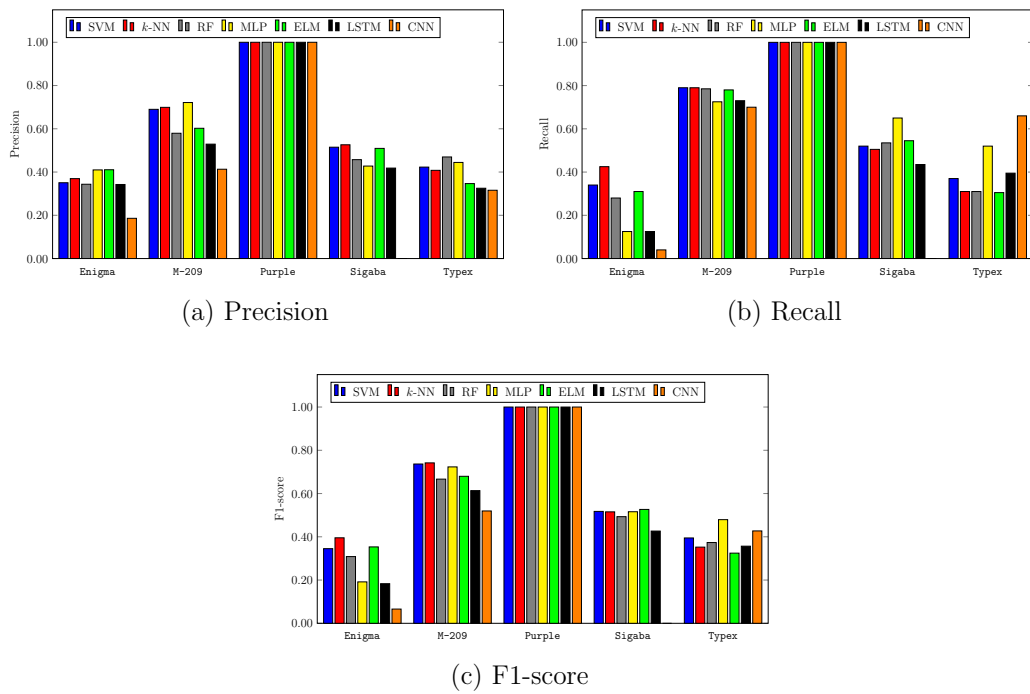
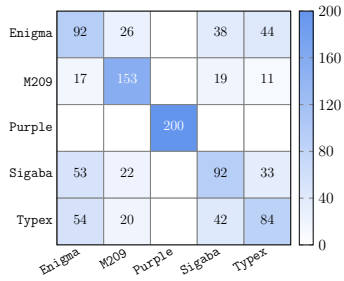
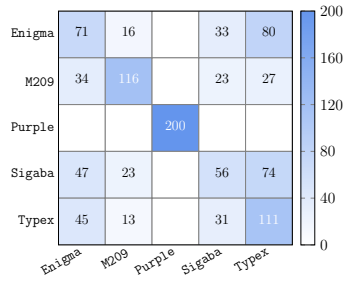


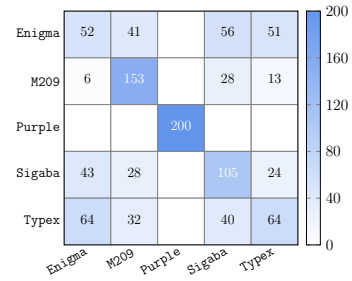
Figure 33: Random-fixed precision, recall, and F1-scores for histogram features



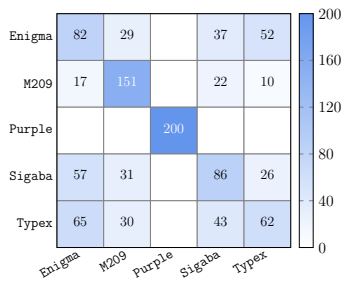
(a) SVM



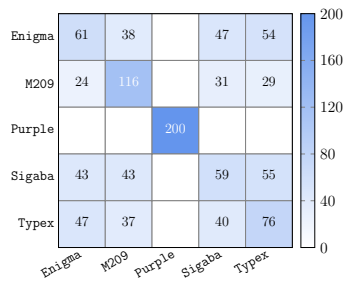
(b)  $k$ -NN



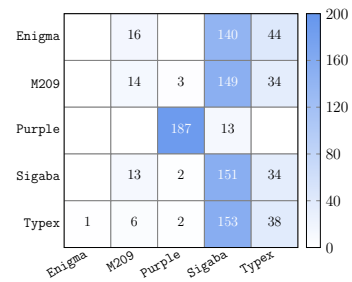
(c) RF



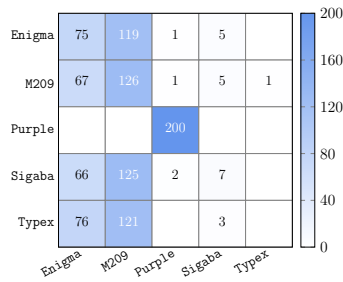
(d) MLP



(e) ELM



(f) LSTM



(g) CNN

Figure 34: Random-fixed confusion matrices for digram features

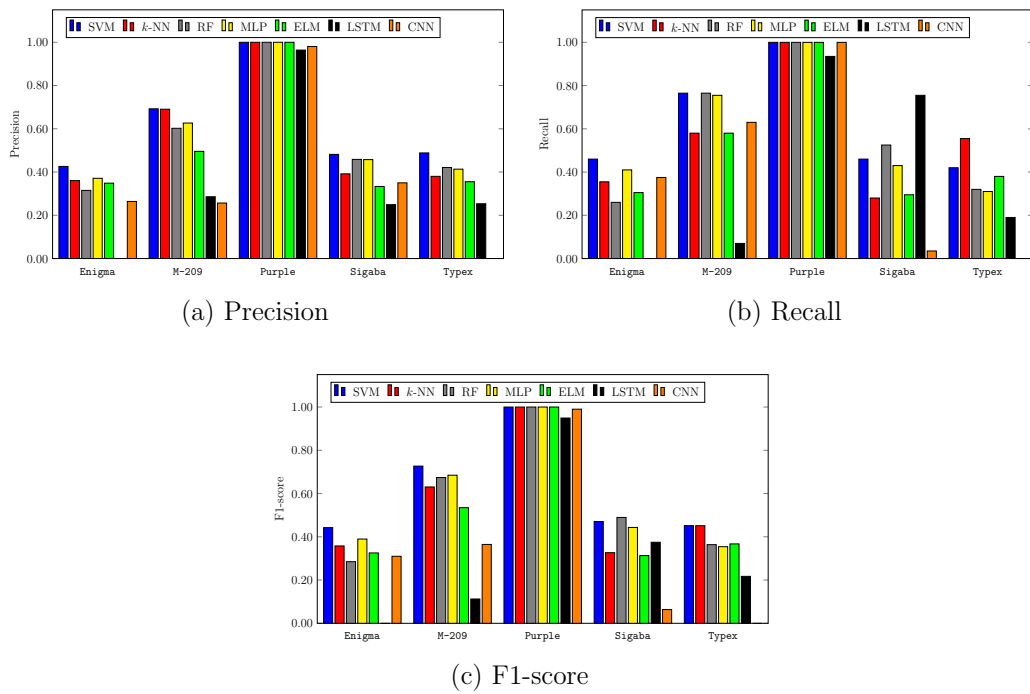


Figure 35: Random-fixed precision, recall, and F1-scores for digram features

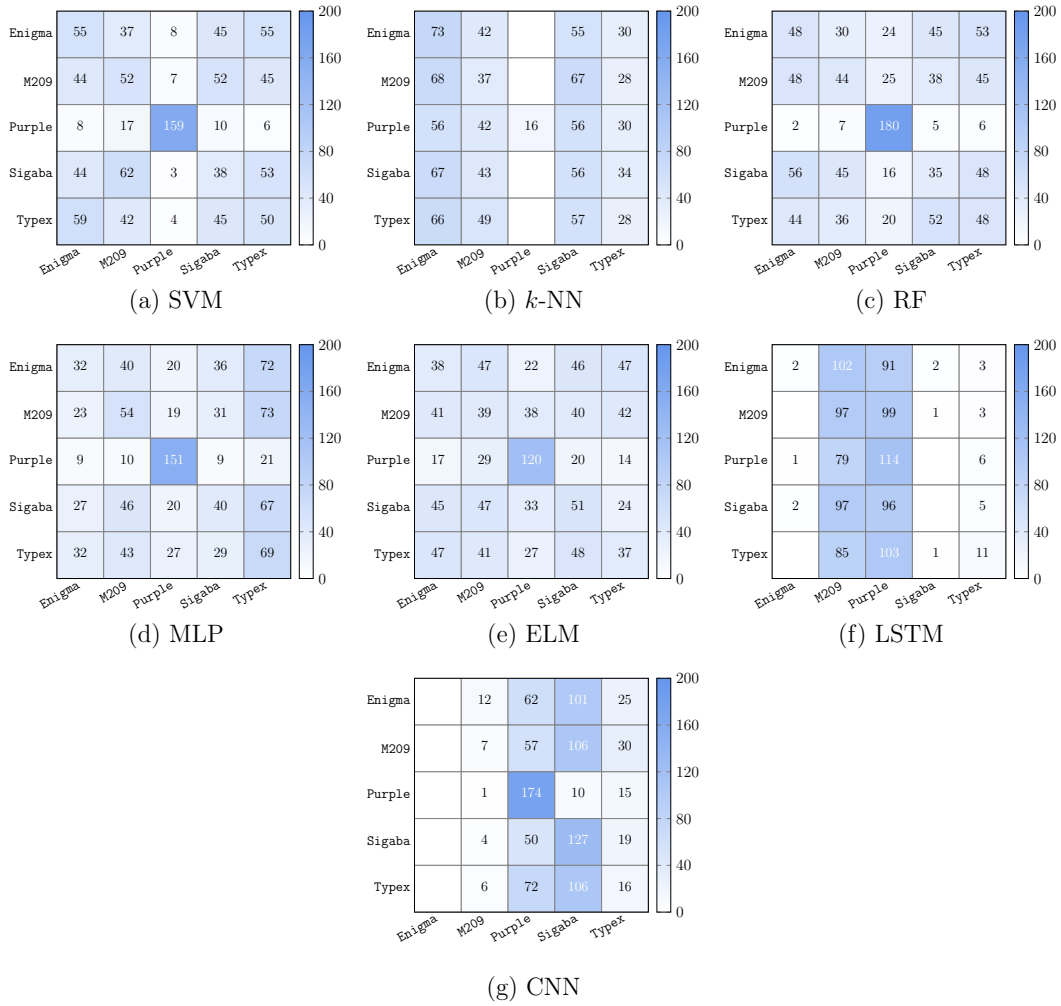


Figure 36: Random-fixed confusion matrices for letter sequence feature



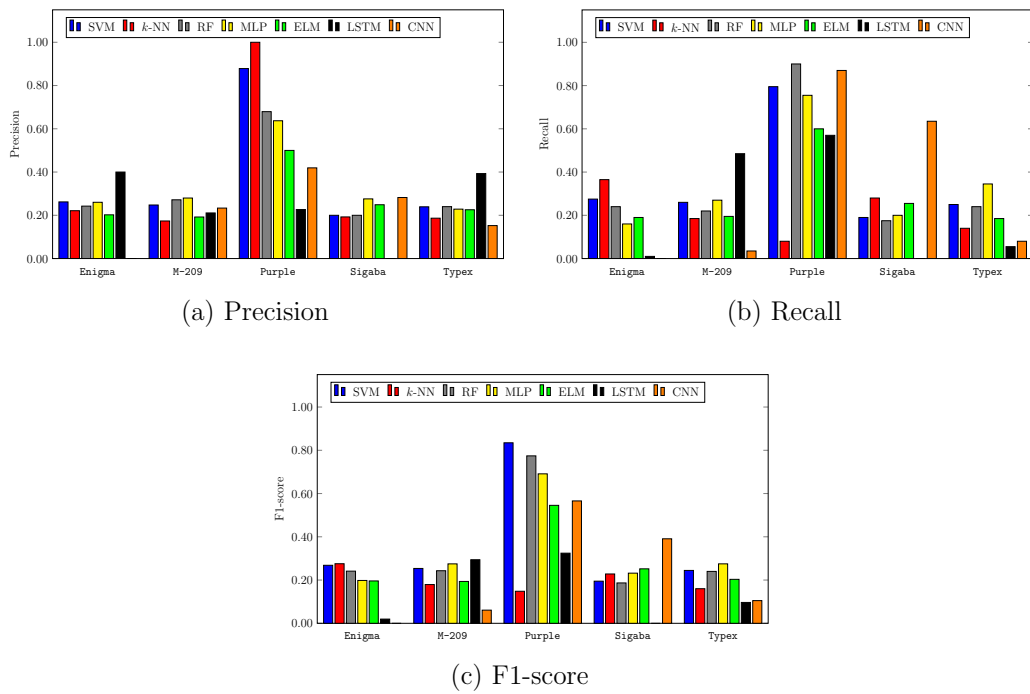


Figure 37: Random-fixed precision, recall, and F1-scores for letter sequence features

## Summary of Results for Fixed-Random Scenario

In this section, we give results for the fixed-random scenario, which is discussed in Section 3.3.3. We experiment with each of the seven models (SVM,  $k$ -NN, RF, MLP, ELM, LSTM, and CNN) using each of the three feature types (histogram, digram, and letter sequence) for a total of 21 distinct models. For each model, we provide a confusion matrix, and we give the precision, recall, and F1-score for each of the five ciphers in bar graph form. The confusion matrices and bar graphs for the histogram features appear in Figures 38 and 39, respectively; the confusion matrices and bar graphs for the digram features are in Figures 40 and 41, respectively; and the confusion matrices and bar graphs for the letter sequence features are in Figures 42 and 43.

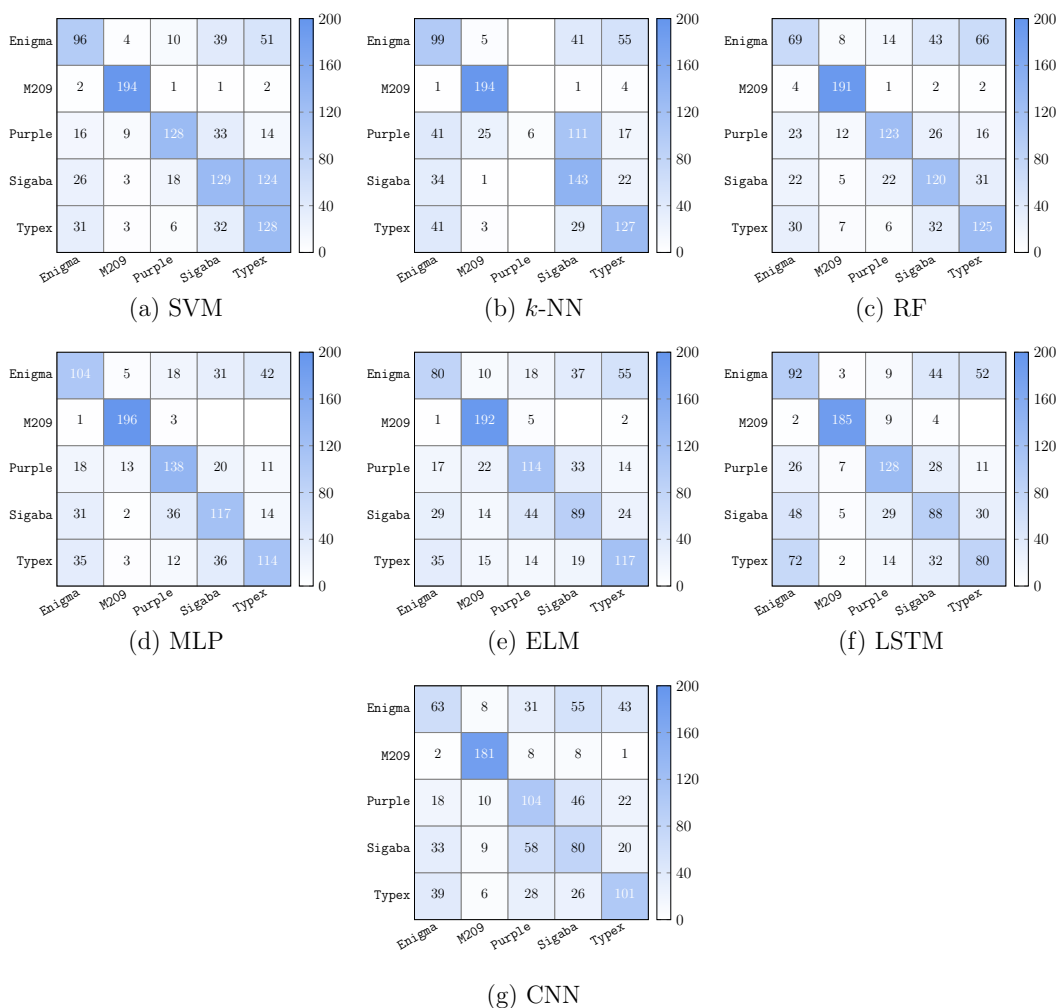


Figure 38: Fixed-random confusion matrices for histogram features

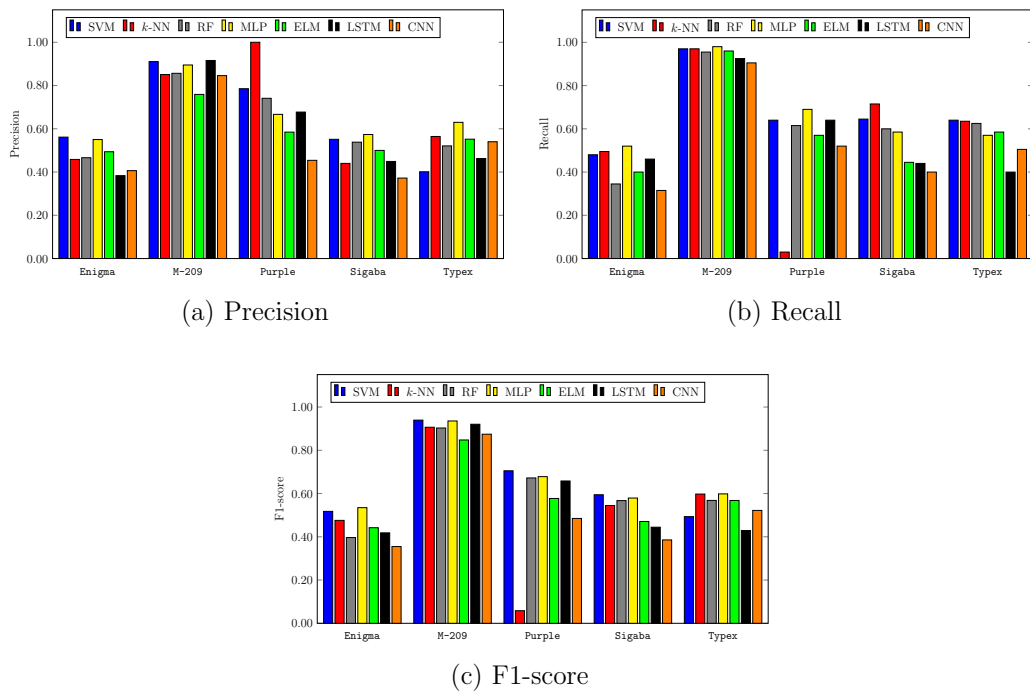
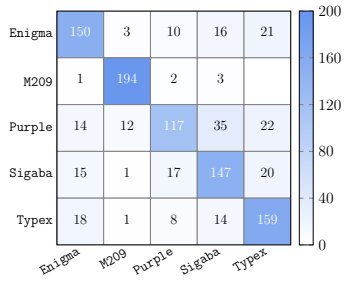
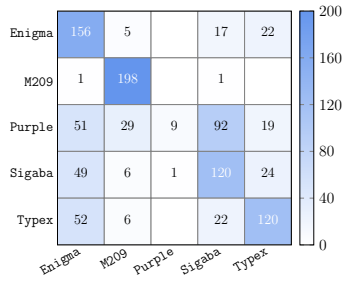


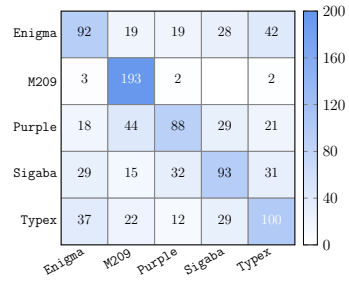
Figure 39: Fixed-random precision, recall, and F1-scores for histogram features



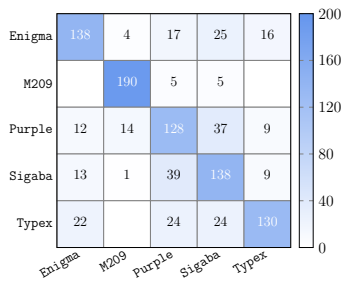
(a) SVM



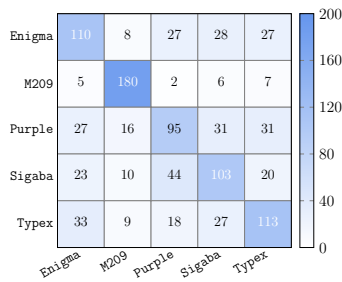
(b)  $k$ -NN



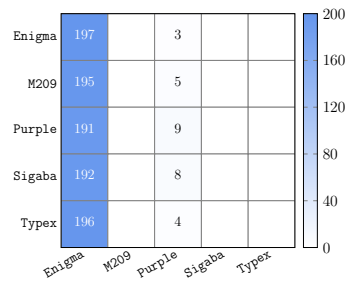
(c) RF



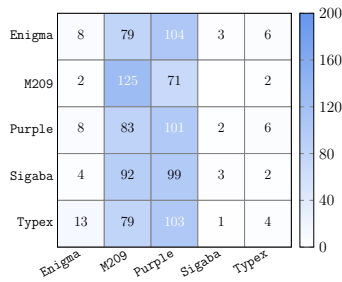
(d) MLP



(e) ELM



(f) LSTM



(g) CNN

Figure 40: Fixed-random confusion matrices for digram features

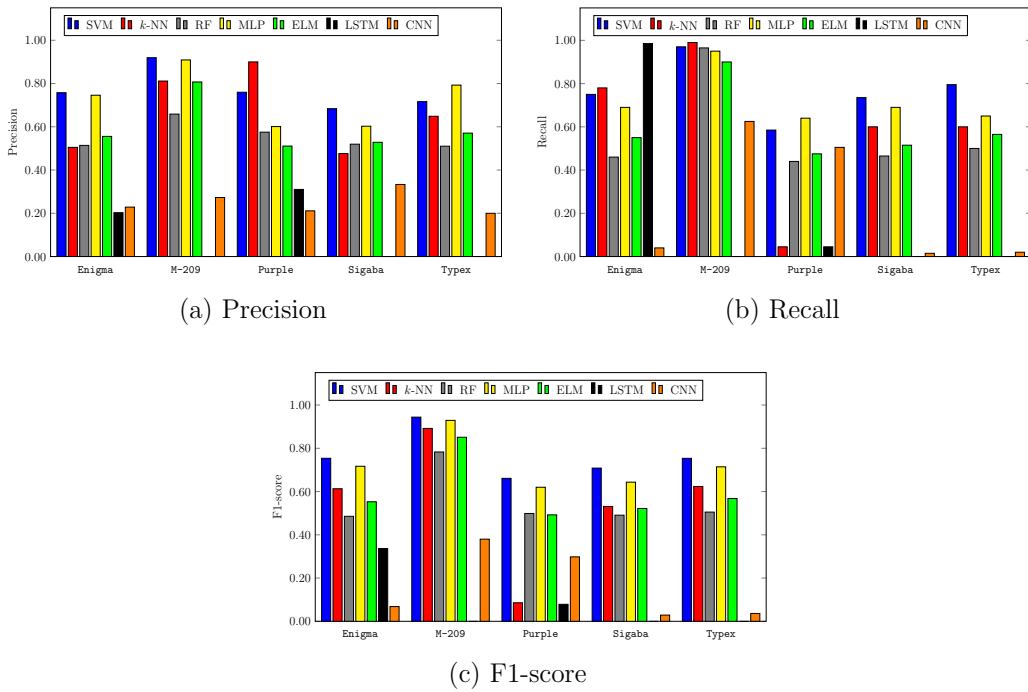


Figure 41: Fixed-random precision, recall, and F1-scores for digram features

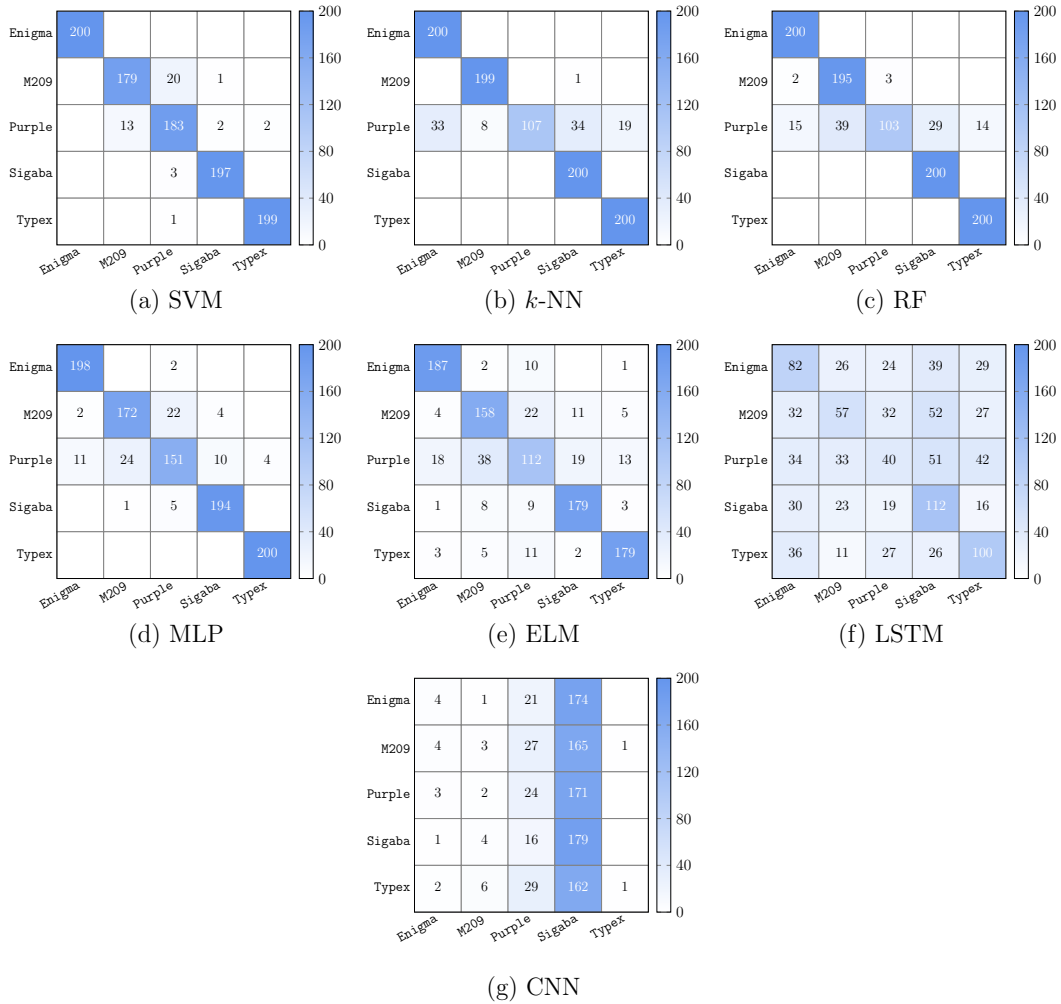


Figure 42: Fixed-random confusion matrices for letter sequence feature

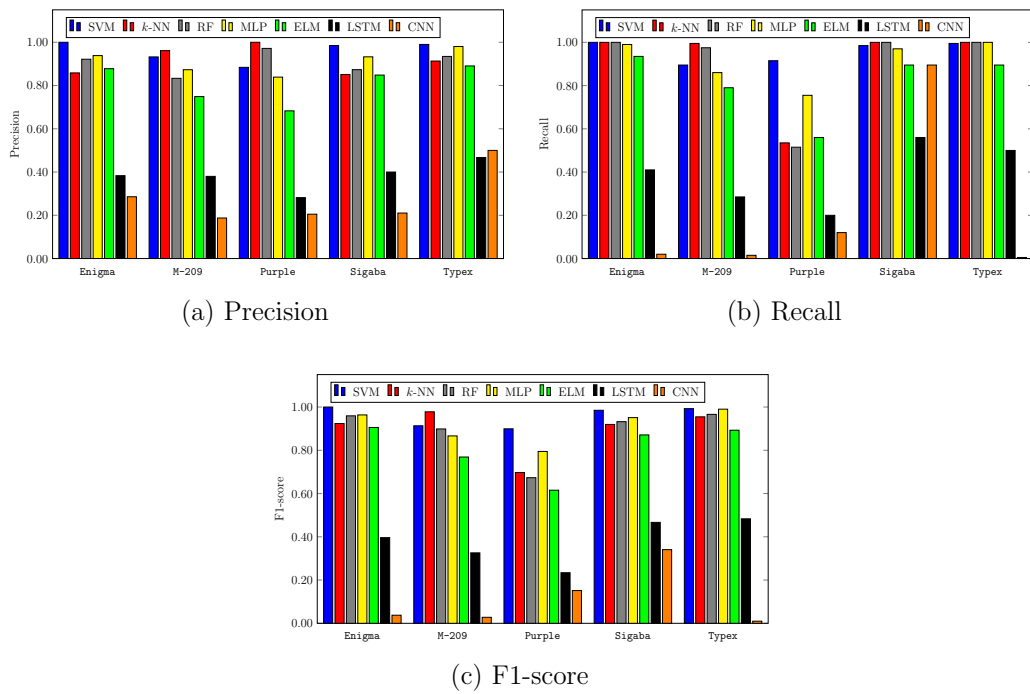


Figure 43: Fixed-random precision, recall, and F1-scores for letter sequence features